Geoscience Frontiers 10 (2019) 195–212

HOSTED BY

Contents lists available at ScienceDirect

China University of Geosciences (Beijing)

Geoscience Frontiers

journal homepage: www.elsevier.com/locate/gsf

Research Paper

Ages and Hf isotopes of detrital zircons from the Permian strata in the Bengbatu area (Inner Mongolia) and tectonic implications

Bing Xu [a], Guochun Zhao [a,b,*], Jianhua Li [b,c], Dongxing Liu [a], Bo Wang [b], Yigui Han [b], Paul R. Eizenhöfer [d], Xiaoran Zhang [b], Wenzhu Hou [b], Qian Liu [b]

[a] State Key Laboratory of Continental Dynamics, Department of Geology, Northwest University, Xi'an 710069, China
[b] Department of Earth Sciences, The University of Hong Kong, Pokfulam Road, Hong Kong, China
[c] Institute of Geomechanics, Chinese Academy of Geological Sciences, Beijing 100081, China
[d] Department of Geology and Environmental Science, University of Pittsburgh, Pittsburgh, PA, USA

ARTICLE INFO

Article history:
Received 22 April 2018
Received in revised form
26 July 2018
Accepted 13 August 2018
Available online 30 August 2018
Handling Editor: M. Santosh

Keywords:
Detrital zircon
U-Pb dating
Hf isotope
Central Asian Orogenic Belt
Subduction
Back-arc basin

ABSTRACT

The Central Asian Orogenic Belt (CAOB) was built up through protracted accretion and collision of a variety of terranes/micro-continents during Neoproterozoic–Mesozoic time. To understand potential links among Paleozoic subduction and accretionary processes that were operative during the development of the southeastern CAOB, we conducted a combined U-Pb and Hf-isotope analysis of detrital zircons from previously defined Devonian, Carboniferous and Early Permian strata in the Bengbatu area, Inner Mongolia. Detrital zircons from (meta-) sandstones in these strata commonly yield major Paleozoic age populations at ca. 300–261 Ma, 351–300 Ma and 517–419 Ma, and also give several Precambrian ages that range from 2687 Ma to 544 Ma. The youngest ages redefine the deposition of all these strata to be in the Middle Permian (Wordian–Capitanian) or later, much younger than previously considered. These ages, coupled with regional magmatic records, support an interpretation of most surrounding areas as possible detritus sources, including the Mongolian arcs to the north, the Northern Accretionary Orogen to the south, and the intervening Erenhot–Hegenshan Ophiolite Belt. Zircons with magmatic ages of ca. 500–350 Ma and ca. 300–261 Ma display a large range of $\varepsilon_{Hf}(t)$ values (−13.97 to +15.31), whereas ca. 350–300 Ma zircons are dominated by positive $\varepsilon_{Hf}(t)$ values (+0.14 to +16.00). These results support the occurrence of two significant shifts of the zircon $\varepsilon_{Hf}(t)$ values, which has tectonic implications for the understanding of the Carboniferous–Permian evolution of the southeastern CAOB. A marked shift from mixed to positive zircon $\varepsilon_{Hf}(t)$ values at 350–330 Ma likely manifests the incipient opening of the Hegenshan Ocean, due to the slab rollback of the subducting Paleo-Asian Oceanic lithosphere. Another shift from positive to mixed zircon $\varepsilon_{Hf}(t)$ values at ca. 300 Ma likely corresponds to a tectonic switch from syn-orogenic subduction-related to post-orogenic extensional setting, genetically related to the tectonic collapse of a formerly overthickened crust.

1. Introduction

The Central Asian Orogenic Belt (CAOB) is one of the largest accretionary orogenic collages in the world (e.g., Sengör et al., 1993; Xiao et al., 2003, 2009a, b; Windley et al., 2007). It is bounded to the north by the Siberian craton, to the west by the East European block and to the south by the Tarim and North China cratons (Fig. 1). This vast orogenic belt was built up through Neoproterozoic–Mesozoic accretion and collision of a series of terranes, including island arcs, seamounts, fore-arc and back-arc basins, and micro-continents (Wang and Liu, 1986; Sengör and Natal'in, 1996a, b; Xu and Chen, 1997; Xiao et al., 2003, 2004, 2009a, b, 2010, 2015; Kröner et al., 2011; Xu et al., 2013; Xiao and Santosh, 2014; Han et al., 2015, 2016a, b; Chen et al., 2017a). The accretionary and collisional processes, starting at ~750 Ma and lasting till Early Triassic time, resulted in (1) the closure of the Paleo-Asian Ocean (PAO) (Xiao et al., 2003, 2009a, b, 2013, 2015; Eizenhöfer et al., 2014; Han et al., 2015; Zhang et al., 2015a; Zhu et al., 2015), (2) the assembly of Eurasia, including the amalgamation of the Tarim and North

* Corresponding author. Fax: +853 25176912.
E-mail address: gzhao@hku.hk (G. Zhao).
Peer-review under responsibility of China University of Geosciences (Beijing).

https://doi.org/10.1016/j.gsf.2018.08.003

Figure 1. Tectonic subdivision of central and east Asia showing the Central Asian Orogenic Belt and surrounding major cratons/blocks (modified after Li, 2006). A square outlines the position of Fig. 2.

China cratons in the south, the East European and Siberian blocks in the north, and some microcontinents, terranes and arcs in or between the blocks (Heubeck, 2001; Torsvik and Cocks, 2004), and (3) considerable Phanerozoic juvenile crustal growth (Sengör et al., 1993; Eizenhöfer et al., 2015b).

Despite much advancement made in understanding of formation and evolution of the CAOB, several issues continue to be uncertain, especially regarding when and how the Paleo-Asian Ocean subducted and closed to assemble the Eurasia. Competing tectonic models emphasizing different accretionary processes include: (1) progressive subduction and accretion associated with the closure of a single major ocean (e.g., Sengör et al., 1993; Sengör and Natal'in, 1996a, b; Yakubchuk, 2004), (2) accretion of several complexes onto continental margins or within oceanic domains (e.g., Mossakovsky et al., 1993; Fedorovskii et al., 1995), and (3) punctuational subduction and collision among several micro-continents and arcs with bidirectional subduction polarity (e.g., Xiao et al., 2003, 2009a, b; Briggs et al., 2007; Windley et al., 2007; Kelty et al., 2008). In addition, controversy has focused on the timing of final closure of the Paleo-Asian Ocean, with some researchers invoking that the ocean has been closed since Late Devonian to Early Carboniferous time (e.g., Tang, 1990; Shao, 1991; Xu and Chen, 1997), whereas others argue that the ocean was not closed

until the Late Permian to Early Triassic (e.g., Hsü et al., 1991; Sengör et al., 1993; Xiao et al., 2003, 2009a; Miao et al., 2008; Eizenhöfer et al., 2014, 2015a).

In southeastern CAOB, the Erenhot-Hegenshan Ophiolite Belt occupies an intermediate position between two terranes termed the Northern Accretionary Orogen and the Uliastai Continental Margin (Fig. 1; Jian et al., 2008, 2010; Eizenhöfer et al., 2014). This belt records wealthy information regarding how the two terranes amalgamated, and is crucial for differentiating among the above-stated models and understanding the architecture of southeastern CAOB. Important processes operating in the southeastern CAOB systems include crustal shortening and retro-arc foreland basin development, ophiolite emplacement, arc-related and post-orogenic magmatism, crustal extension and back-arc basin development (e.g., Chen et al., 2000; Shi et al., 2003, 2004; Miao et al., 2008; Jian et al., 2008, 2012; Xu et al., 2013; Zhang et al., 2014; Tong et al., 2015; Hu et al., 2015). Although most of these processes have been well understood in their own right, the potential links and feedbacks among them remain unclear, especially on (1) how tectono-magmatism evolved in response to the development of the inferred Hegenshan Ocean from ophiolites during the subduction of the Paleo-Asian Ocean (Robinson et al., 1995, 1999; Miao et al., 2008; Eizenhöfer et al., 2015a); and (2) how events in the retro-arc/back-arc, arc, and fore-arc related to each other.

Detrital zircons are physically robust records that serve well to trace magmatic evolution of provenance terranes, and to establish the linkage between major terranes by comparing age distributions (Cawood et al., 2012). Zircon Hf isotopic systematics has been proven particularly useful in distinguishing between orogenic processes dominated by the reworking of ancient crust and those dominated by additions of juvenile crust (Collins et al., 2011). In this study, a combined U-Pb and Hf-isotope analysis of detrital zircons has been conducted in Permian strata of the Bengbatu area, western Erenhot-Hegenshan Ophiolite Belt. The Permian strata are chosen because the detrital zircons therein potentially contain more comprehensive magmatic records than those from any older strata. The reported detrital zircon age patterns and variations in Hf isotopic ratios provide new insights into Paleozoic multiple subduction and accretionary processes that combined to build southeastern CAOB.

2. Geological background and sample descriptions

2.1. Regional geology

The CAOB in Chinese Inner Mongolia, also termed "Manchurides" (Sengör and Natal'in, 1996a, b) or "Great Xinganling-Inner Mongolian orogenic belt" (Yin and Nie, 1996), is an ENE-trending tectonic collage composed of micro-continents, arcs, accretionary complexes, and remnants of ophiolites (Xiao et al., 2003, 2009a, b; Shi et al., 2003; Li et al., 2011; Jian et al., 2012; Xu et al., 2013; Zhao et al., 2014). In the Inner Mongolia, the CAOB can be divided into five litho-tectonic units. They are, from south to north, the Southern Accretionary Orogen, the Solonker Suture Zone, the Northern Accretionary Orogen, the Erenhot-Hegenshan Ophiolite Belt, and the Uliastai Continental Margin (Fig. 2). The Southern Accretionary Orogen comprises the Bainaimiao arc and the Ordor Sum complex;

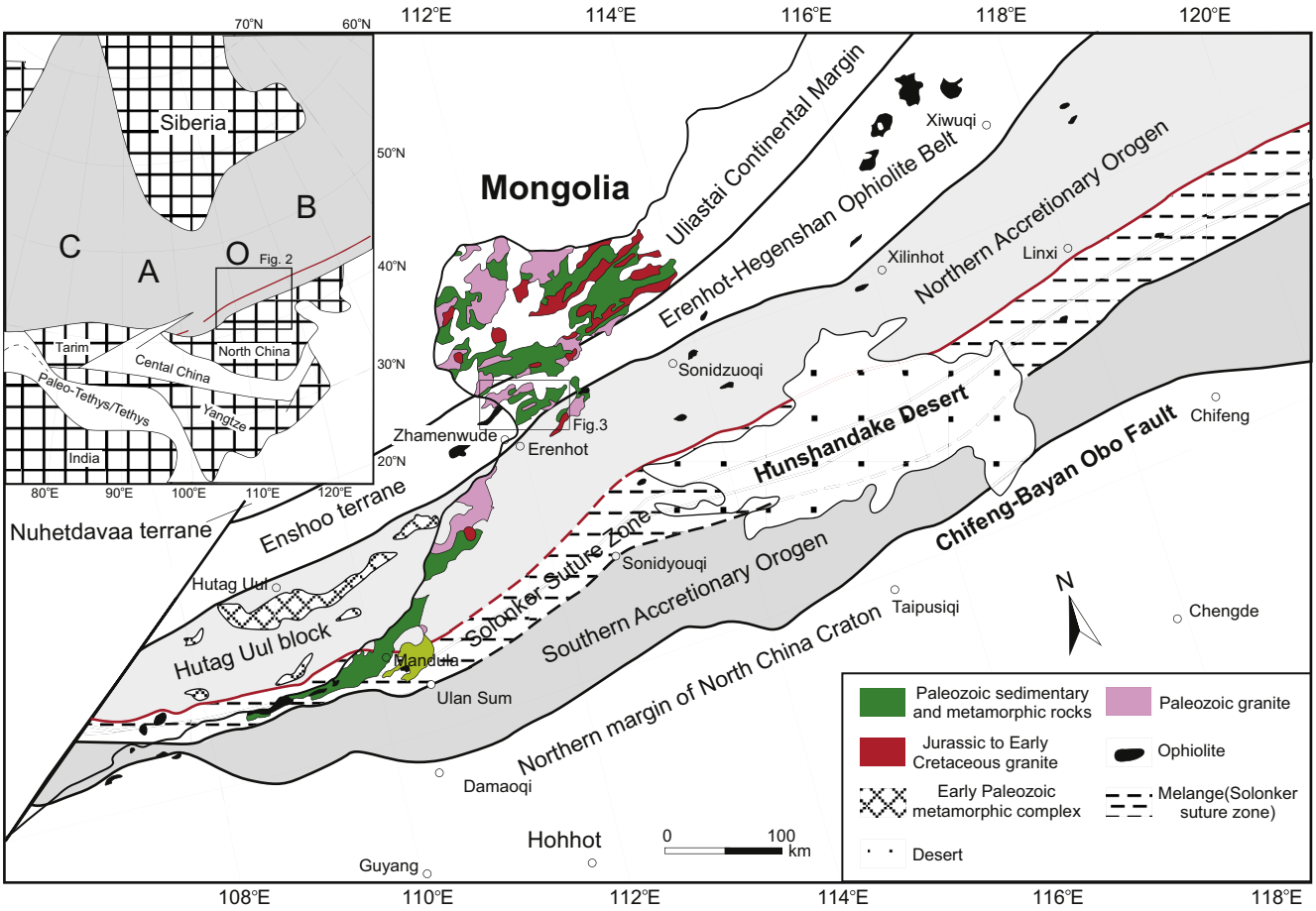

Figure 2. Geological sketch map of the southeastern CAOB (modified after IMBGMR, 1991; Xiao et al., 2009b; Jian et al., 2010).

the former is composed of calc-alkaline tholeiitic basalts, minor felsic lavas and granitoids (Shao, 1989; Nie and Bjørlykke, 1999; Zhang et al., 2014), whereas the latter consists of ophiolites, high-pressure metamorphic rocks and granitic gneisses (Wang and Liu, 1986; Xiao et al., 2003; Li, 2006; Miao et al., 2007). The Solonker Suture Zone, marked by extensive outcrops of Permian–Early Triassic ophiolites (Wang and Liu, 1986; Miao et al., 2007; Jian et al., 2008), is considered as the site of final closure of the eastern segment of the Paleo-Asian Ocean (Eizenhöfer et al., 2014). The Northern Accretionary Orogen, extending westward into the Hutag Uul block in Mongolia, consists of several accretionary and metamorphic complexes, including the Baolidao and Xilinhot complexes (Shi et al., 2003; Chen et al., 2009). The Baolidao complex, formed in the Late Carboniferous, consists of gabbroic diorite, quartz diorite, tonalite and granodiorite (Chen et al., 2000, 2009; Miao et al., 2007; Xu et al., 2013). The Xilinhot complex, extending for ~150 km from Erdaojing to Honger, consists of schist, paragneiss, orthogneiss, amphibolite and ultramafic rocks (Shi et al., 2003; Li et al., 2011). The Erenhot-Hegenshan Ophiolite Belt contains several ophiolitic fragments, which are composed of dunite, gabbro, sheeted dikes, tholeiitic pillow basalt, radiolarian chert and coral limestone (Tang, 1990; Tang and Yan, 1993). The ophiolitic rocks are overlain by ~10 km thick Carboniferous–Permian transgressive sequences, which represent post-collisional sedimentation following the closure of the Hegenshan ocean (IMBGMR, 1991; Shen et al., 2006). Recent recognition of ~354 Ma gabbros in the north Hegenshan and east Erenhot led many authors (e.g. Jian et al., 2012; Zhang et al., 2015c) to infer that the Hegenshan Ophiolite Belt extends further to the west, through the Erenhot into Mongolia. The Uliastai Continental Margin lies between Erenhot and Uliastai, and may extend westward into the Nuhetdavaa terrane in Mongolia as part of the Mongolian arcs (Badarch et al., 2002; Eizenhöfer et al., 2015a, b). The basement of the Uliastai Continental Margin is composed of Proterozoic gneiss, schist, and quartzite. The basement rocks were unconformably overlain by Paleozoic sedimentary rocks, which were extensively intruded by Devonian to Carboniferous arc-related, calc-alkaline and alkaline magmatic rocks, indicating that the Uliastai Continental Margin evolved into an active continental margin in Devonian–Carboniferous time (Badarch et al., 2002; Xiao et al., 2003).

2.2. Stratigraphy of the Bengbatu area

The Bengbatu area, located ~35 km to the northeast of Erenhot, represents the western terminal of the Erenhot-Hegenshan Ophiolite Belt in China (Fig. 2). The area is characterized by widespread Permo–Carboniferous volcano-sedimentary rocks that unconformably overlie the Devonian strata. The Devonian strata are composed of quartz schist, tuff, silicic slate, siltstone, and limestone lenticles (Fig. 3; IMBGMR, 1991; Li et al., 1996). The Carboniferous strata contain the Benbatu Formation in the lower part and the Amushan Formation in the upper part (IMBGMR, 1965, 1991). The Benbatu Formation is composed of greywacke, sandstone, siltstone, tuff and andesite, depositing in a shallow marine environment (IMBGMR, 1965, 1991). The Amushan Formation is characterized by a fining-upward sedimentary succession that comprises conglomerate, pebbly greywacke, feldspathic sandstone, laminated siltstone, and interbedded tuff, andesite and limestone (IMBGMR, 1965, 1991; Yang et al., 2015). The Permian strata, characterized by clastic-volcanic rock assemblages, can be divided into two series, i.e., the Early Permian Baoligaomiao Formation and the Middle to Late Permian Zhesi Formation (IMBGMR, 1965, 1991; Shao et al., 2014; Fig. 4). The Baoligaomiao Formation, about 1.2 km thick, is composed of tuffaceous/carbonaceous/sandy slate, tuff, andesite and sandstone. The Zhesi Formation, about 1.5 km thick, is composed of conglomerate, sandstone, greywacke and minor tuffaceous rocks in the lower part, and slate, shale, tuff, sandstone and interbedded fossiliferous limestone in the upper part. The above-stated Devonian–Permian rock sequences were intruded by Carboniferous to Early Cretaceous plutons (IMBGMR, 1991; Meng, 2003; Wang et al., 2011; Daoudene et al., 2012). Recently, an Early

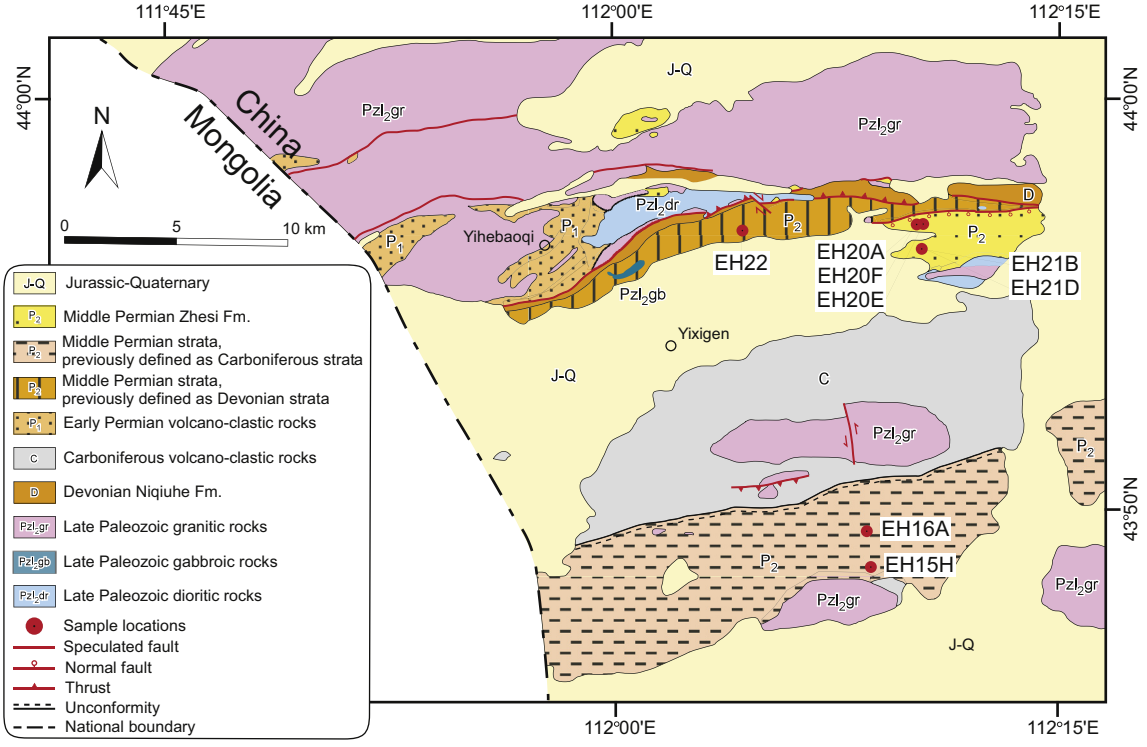

Figure 3. Simplified geological map of the Bengbatu area (after IMBGMR, 1965, 1991). Sample locations are shown.

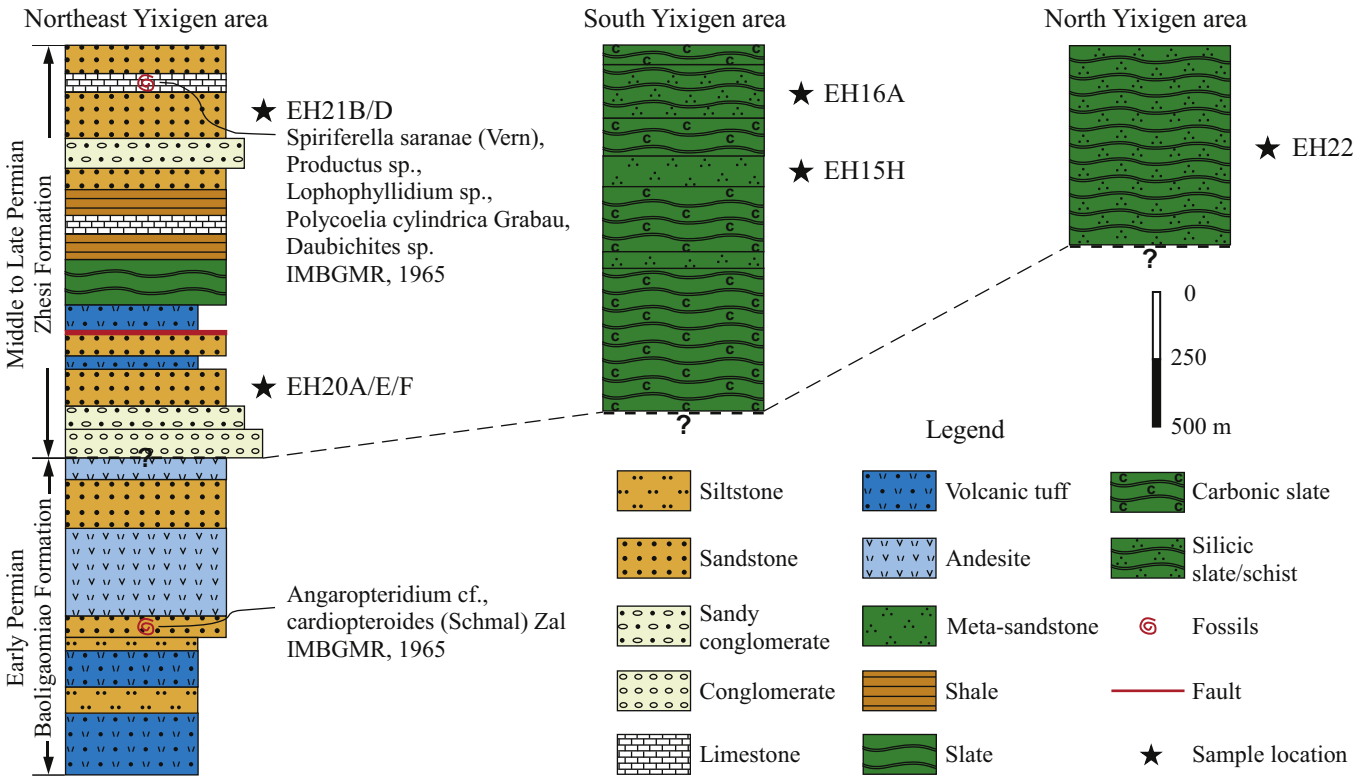

Figure 4. Stratigraphic column of the Permian strata in the Bengbatu area (modified after IMBGMR, 1965, 1991). The sample locations are shown on the stratigraphic column.

Carboniferous (ca. 353–345 Ma) ophiolitic suite was recognized ~40 km to the southeast of the study area and is composed of serpentinized ultramafic rocks, gabbros, mafic lavas and minor plagiogranite dikes, probably forming in a back-arc tectonic setting (Zhang et al., 2015c).

2.3. Sample descriptions

Eight rock samples were collected from the previously defined Devonian, Carboniferous and Early Permian strata. Their locations are shown in Figs. 3 and 4.

Two rock samples (EH16A and EH15H) were collected from the southern part of the Bengbatu area. Sample EH16A is a fine lithic arenite composed principally of quartz (~40%–45%), feldspar (~20%–25%) and rock fragments (~27%, mainly igneous type) (Fig. 5a and b). Sample EH15H is a dark gray meta-sandstone, containing quartz (~5%), lithic fragments (~25%), feldspar (~25%–30%) and alteration products (~30%–40%) such as epidote and chlorite (Fig. 5c and d). The two samples are characterized by pervasive development of salty cleavages (Fig. 5a and c), which accommodate shortening via pressure solution.

Five rock samples were collected from the Permian Zhesi Formation in the northern Bengbatu area (Fig. 3). Among them, three samples (EH20A, EH20E and EH20F) are grayish-red fine to medium lithic arenites, dominantly composed of moderate quartz (~20%–25%), abundant rock fragments (~40%–55%) and low to moderate feldspar (~8%–15%) (Fig. 5e and f). The remaining two samples (EH21B and EH21D) are bedded russet fine feldspathic arenites, and consist primarily of immature-textured quartz (~15%–20%), abundant feldspar (~45%–55%), moderate lithic fragments (~20%–22%) and minor biotite (~1%–3%) (Fig. 5g and h).

Sample EH22 is a strongly foliated meta-sandstone composed of quartz (~70%–78%) and mica (~15%–18%) (Fig. 5i and j). Within the sample, the foliation is prominent and defined by planar arrangement of biotites, elongated quartz aggregates, and compositional layering (Fig. 5j).

3. Analytical methods

3.1. Sample preparation

Zircon grains were handpicked under a binocular microscope from heavy minerals of samples processed by conventional crushing, heavy-liquid and magnetic separation techniques at the Langfang Regional Geological Survey, Hebei Province, China. Randomly selected zircon grains were mounted in epoxy resin and polished to expose their interior. Zircons were then photographed under transmitted and reflected light through optical microscope. Cathodoluminescence (CL) imaging was performed on a FEI Quanta 400 FEG environmental scanning electron microscope equipped with an Oxford energy dispersive spectroscopy and a Gatan CL3+ detector at the Northwest University in Xi'an, China. The obtained CL images reveal the internal structures of zircons and indicate potential target sites for U-Pb analysis.

3.2. Zircon U-Pb geochronology

Zircon U-Pb dating was carried out using a laser ablation-inductively coupled plasma-mass spectrometry (LA-ICP-MS) instrument at the State Key Laboratory of Continental Dynamics at the Northwest University in Xi'an, China. The LA-ICP-MS was assembled by an ArF-excimer 193 nm laser ablation system (GeoLas 200M, MicroLas, Germany) and a quadrupole ICP-MS (Agilent 7500a). Laser spot size was between 30 μm and 40 μm, and laser frequency was 10 Hz. High-purity helium was used as carrier gas, which was mixed with a make-up gas of high-purity argon before

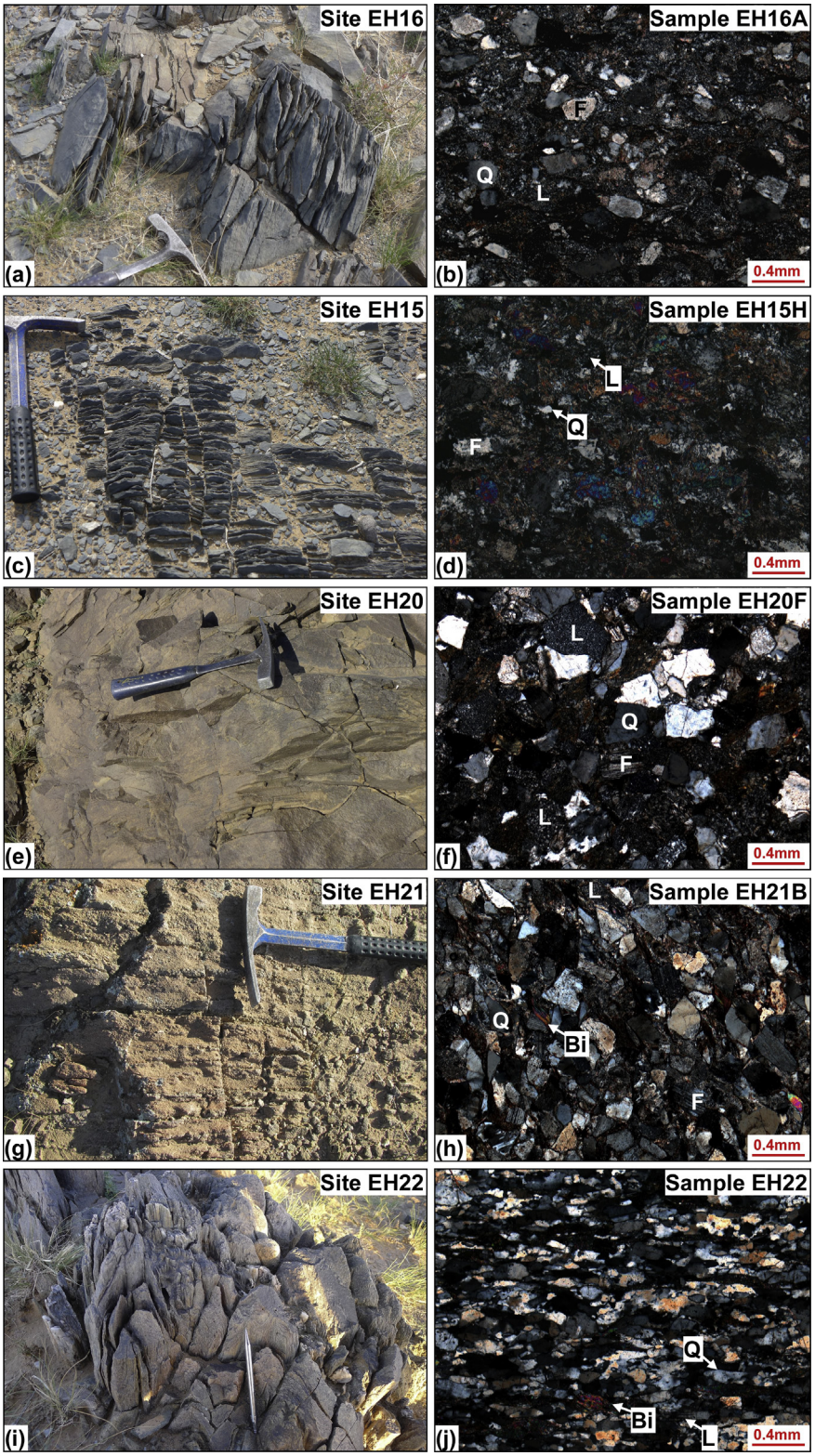

Figure 5. Field and microscopic pictures of representative rocks from the sedimentary strata in the Bengbatu area. Abbreviations: Q–quartz; F–feldspar; L–lithic fragment; Bi–Biotite.

entering the ICP-MS to achieve stable and optimum conditions, resulting in negligible contribution of ^{204}Hg to ^{204}Pb (count rate of the mass 204 for blank <100 counts per second). Detailed instrumental settings and analytical procedures refer to Diwu et al. (2012) and Liu et al. (2008).

Off-line raw data were processed using the ICPMSDataCal 8.6 program (Liu et al., 2010b) to obtain U-Th-Pb isotopic ratios and elemental concentrations. The Harvard zircon 91500 was used as a standard for isotopic ratio correction. Concentrations of U, Th and Pb were calculated by using NIST 610 as an external standard and

^{29}Si as an internal standard. Zircon standard GJ-1 was analyzed as an unknown and yielded a weighted mean ^{206}Pb/^{238}U age of 601.3 ± 1.0 Ma (MSWD = 1.7, n = 64), which is in good agreement with the recommended TIMS age of 600.4 ± 0.6 Ma (Jackson et al., 2004). In all analyzed zircon grains, the common Pb correction was not necessary due to the low signal of common ^{204}Pb and high ^{206}Pb/^{204}Pb. Isoplot (ver. 3.23) program (Ludwig, 2003) was used to plot concordia diagrams and probability density distribution plots, and for age calculations. ^{206}Pb/^{238}U ages were used for zircons younger than 1.0 Ga, while ^{207}Pb/^{206}Pb ages were used for ones older than 1.0 Ga. The analytical data are presented on U-Pb concordia diagrams with 2σ errors.

3.3. Zircon Hf isotopic analysis

Zircon Hf isotopes were determined using a 193 nm Ar-F excimer laser ablation system (RESOlution M-50-LR) attached to a multi-collector ICPMS (Neptune Plus) at the Guangzhou Institute of Geochemistry, Chinese Academy of Sciences (CAS), China. The concordant zircons were selected, and zircon Lu-Hf isotope analyses were conducted on them, targeting the pits generated by U-Pb analyses. Helium was used as the carrier gas during laser ablation. A beam diameter of 45 μm and a pulse rate of 6 Hz were used during laser ablation with a surface energy density approximate to 80 mJ/cm^2. Ablation time for each analysis was 29 s. Detailed analytical procedures and principles of isobaric interference corrections are documented in Wu et al. (2006). Penglai standard zircons used as reference material were measured to check instrument reliability and stability, and yielded an average ^{176}Hf/^{177}Hf ratio of 0.282890 ± 0.000010 (1 standard deviation, n = 73). The result is comparable within errors to the reference value of 0.282906 ± 0.000010 recommended by Li et al. (2010).

Zircon initial ^{176}Hf/^{177}Hf ratios were calculated using measured ^{176}Lu/^{177}Hf and ^{176}Hf/^{177}Hf ratios and ^{176}Lu decay constant of 1.867×10^{-11} yr^{-1} (Söderlund et al., 2004). To calculate $\varepsilon_{Hf}(t)$ values, we adopted a present-day ^{176}Lu/^{177}Hf value of 0.0332 and a ^{176}Hf/^{177}Hf value of 0.282772 for the chondritic uniform reservoir (CHUR) (Bouvier et al., 2008). Depleted mantle model ages (T_{DM1}) were calculated with reference to a depleted mantle reservoir having present-day ^{176}Lu/^{177}Hf value of 0.0384 and ^{176}Hf/^{177}Hf value of 0.283251 (Griffin et al., 2004). Crustal model ages (T_{DM2}) were calculated by assuming that the parental magma from which each zircon crystallized was originated from an average continental crust (^{176}Lu/^{177}Hf = 0.015, Griffin et al., 2004) which was derived from the depleted mantle.

4. Results

4.1. Zircon morphology and Th/U ratios

Detrital zircon grains from the eight samples range from 30 to 240 μm in length, and have length/width ratios of 1–6.4 (Fig. 6). These zircons exhibit different grain morphologies: most zircons are euhedral to subhedral; a few zircons are rounded or subrounded, indicating a higher degree of reworking. Based on the cathodoluminescence (CL) images, these zircons can be grouped morphologically into three types: (1) grains with concentric, oscillatory zoning; (2) concentric oscillatory zoned cores with narrow high luminescent, structureless rims; and (3) irregular grains with partially developed crystal faces or planar banded growth zones, similar to those from gabbroic rocks (Fig. 6). Overall, the type (1), (2) and (3) zircons account for ~90%, ~5% and ~5% of all analyzed zircons, respectively (Fig. 6). Most of the type (1) and (3) zircons and oscillatory-zoned cores in type (2) zircons have Th/U ratios of >0.4 (Appendix Table 1), consistent with an igneous origin. The structureless rims in the type (2) zircons represent metamorphic overgrowths on magmatic cores. However, the origin of the metamorphism remains undetermined, as these metamorphic rims are too narrow to be dated. Detailed zircon U-Th-Pb isotopic data are listed in Appendix Table 1. To ensure the efficient quality, U-Pb analyses that show large variations of signals and/or large age discordance (not between 90% and 110%) were discarded.

4.2. Zircon U-Pb ages and Hf isotopes

4.2.1. Lithic arenites from the Zhesi Formation

Total 55 concordant analyses were obtained from the detrital zircons of sample EH20A, and they define a wide range of ^{207}Pb/^{206}Pb (>1.0 Ga) and ^{206}Pb/^{238}U (<1.0 Ga) ages from 2546 Ma to 266 Ma. On the probability density distribution plots, the Paleozoic ages (40 analyses) are prominent and show two major peaks at ~319 Ma and ~420 Ma, and two minor peaks at ~345 Ma and ~459 Ma (Fig. 7a and b). The other 15 analyses yield Precambrian ages, ranging from 2546 Ma to 715 Ma. Among all obtained ages, the youngest age is 266 ± 2 Ma, with discordance of <10%.

Total 73 concordant analyses were conducted on the detrital zircons of sample EH20E, and they show a spread of ^{207}Pb/^{206}Pb and ^{206}Pb/^{238}U ages between 2058 Ma and 273 Ma. Among these zircons, fifty-seven zircons yield Paleozoic ages that are manifested by a major peak at ~304 Ma and two minor peaks at ~401 Ma and ~459 Ma (Fig. 7c and d); sixteen zircons yield Precambrian ages that range from 2058 Ma to 544 Ma. The youngest concordant (discordance<7%) zircon yields an apparent ^{206}Pb/^{238}U age of 273 ± 2 Ma.

A total of 67 concordant analyses were obtained from the detrital zircons of sample EH20F, and they define a wide range of ^{207}Pb/^{206}Pb and ^{206}Pb/^{238}U ages from 2687 Ma to 283 Ma. Of these, 57 concordant analyses of oscillatory-zoned zircons yield Paleozoic ages, which show a major peak at ~331 Ma and minor peaks at ~292–312 Ma, ~351 Ma, ~370 Ma and ~437 Ma (Fig. 7e and f); the remaining 10 analyses give Precambrian ages, ranging from 2687 Ma to 778 Ma. The youngest zircon yields a ^{206}Pb/^{238}U age of 283 ± 2 Ma (discordance <7%).

A total of 144 dated zircons from the above-stated three samples were analyzed for Hf isotopes. These zircons show highly variable $\varepsilon_{Hf}(t)$ values, ranging from −20.61 to +15.31 (Fig. 8a–f). Their initial ^{176}Hf/^{177}Hf ratios range from 0.281012 to 0.282980, corresponding to the depleted mantle two-stage Hf model ages (T_{DM2}) of 3473–423 Ma. Among these Paleozoic zircons, the lowest $\varepsilon_{Hf}(t)$ value (−13.97) occurs in a relatively young zircon with a ^{236}Pb/^{238}U age of 497 Ma (Spot #17 in sample EH20A), corresponding to the lowest ^{176}Hf/^{177}Hf ratio of 0.282075 and the oldest Hf model age (T_{DM2}) of 2340 Ma (Appendix Table 2).

4.2.2. Feldspathic arenites from the Zhesi Formation

A total of 51 concordant analyses were conducted on the detrital zircons of sample EH21B. Similar to other samples from the Zhesi Formation, there are abundant zircons that record Paleozoic ages, forming an age cluster between 472 Ma and 271 Ma with a major peak at ~316 Ma and minor peaks at ~275 Ma, ~333 Ma and ~376 Ma (Fig. 7g and h). Among these Paleozoic ages, the youngest age is 271 ± 2 Ma, with discordance of <9%.

A total of 68 valid ages were obtained from detrital zircons of sample *EH21D*. Among these, almost all zircons give Devonian to Permian (418–265 Ma) ^{206}Pb/^{238}U ages except for one Silurian grain that has a ^{206}Pb/^{238}U age of 445 ± 4 Ma (discordance <5%). Among these ages, the Carboniferous to Permian ages display a major peak at ~319 Ma and two minor peaks at ~286–296 Ma and ~335 Ma (Fig. 7i and j). The youngest age is 265 ± 2 Ma, with discordance of <5%.

Figure 6. Cathodoluminescence (CL) images for detrital zircons from eight rock samples collected from the Bengbatu area.

A total of 73 dated zircons from the above-stated two samples were analyzed for Hf isotopes. Almost all zircons show positive $\varepsilon_{Hf}(t)$ values of 5.66–16.00 except for one spot that has a negative value of −0.55 (spot #15 in sample EH21D) (Fig. 8g and h). Their initial $^{176}Hf/^{177}Hf$ ratios range from 0.282688 to 0.283041, corresponding to the depleted mantle two-stage Hf model ages (T_{DM2}) of 1340–294 Ma. Among these zircons, the lowest $\varepsilon_{Hf}(t)$ value (−0.55) occurs in a young zircon with a $^{236}Pb/^{238}U$ age of 278 Ma (Spot #15 in sample EH21D), corresponding to a relatively low $^{176}Hf/^{177}Hf$ ratio of 0.282891 and the oldest Hf model age (T_{DM2}) of 1340 Ma (Appendix Table 2).

4.2.3. Meta-sandstone (sample EH22) from the north Yixigen area

A total of 47 concordant ages were obtained for meta-sandstone sample (EH22) collected in the north Yixigen area. These ages define a relatively narrow spread of $^{206}Pb/^{238}U$ ages between 496 Ma and 268 Ma (Fig. 9a and b). On the probability density distribution plots, all obtained ages display a major peak at ~302 Ma and a minor peak at ~283 Ma. Among these ages, the youngest age is 268 ± 2 Ma, with discordance of <5%.

A total of 35 dated zircons were analyzed for Hf isotopes. All zircons show positive $\varepsilon_{Hf}(t)$ values of 1.36–11.96 (Fig. 10a). Their initial $^{176}Hf/^{177}Hf$ ratios range from 0.282510 to 0.282949, corresponding to the depleted mantle two-stage Hf model ages (T_{DM2}) of 1376–538 Ma. Among these spots, the lowest $\varepsilon_{Hf}(t)$ value (+1.36) occurs in the oldest zircon with a $^{236}Pb/^{238}U$ age of 496 Ma (Spot #46 in sample EH22), corresponding to the lowest $^{176}Hf/^{177}Hf$ ratio of 0.282510 and the oldest Hf model age (T_{DM2}) of 1376 Ma (Appendix Table 2).

4.2.4. Lithic arenites from the south Yixigen area

Samples EH15H and EH16A are lithic arenites collected from the south Yixigen area. Total 77 concordant ages have been obtained from the detrital zircons of sample EH15H. Similar to other samples from the Zhesi Formation, there are abundant zircons that record late Paleozoic ages, forming a very narrow age cluster between 361 Ma and 288 Ma with a major peak at ~317 Ma and two minor peaks at ~343 Ma and ~303 Ma (Fig. 9c and d). Among these zircons, the youngest zircon yields an apparent $^{206}Pb/^{238}U$ age of 288 ± 2 Ma (discordance <5%).

A total of 63 analyses were conducted on 63 zircon grains from sample EH16A. Of these, 60 concordant analyses yield Paleozoic $^{236}Pb/^{238}U$ ages of 458–261 Ma, which show a major peak at ~277 Ma and two minor peaks at ~305 Ma and ~262 Ma (Fig. 9e and f);

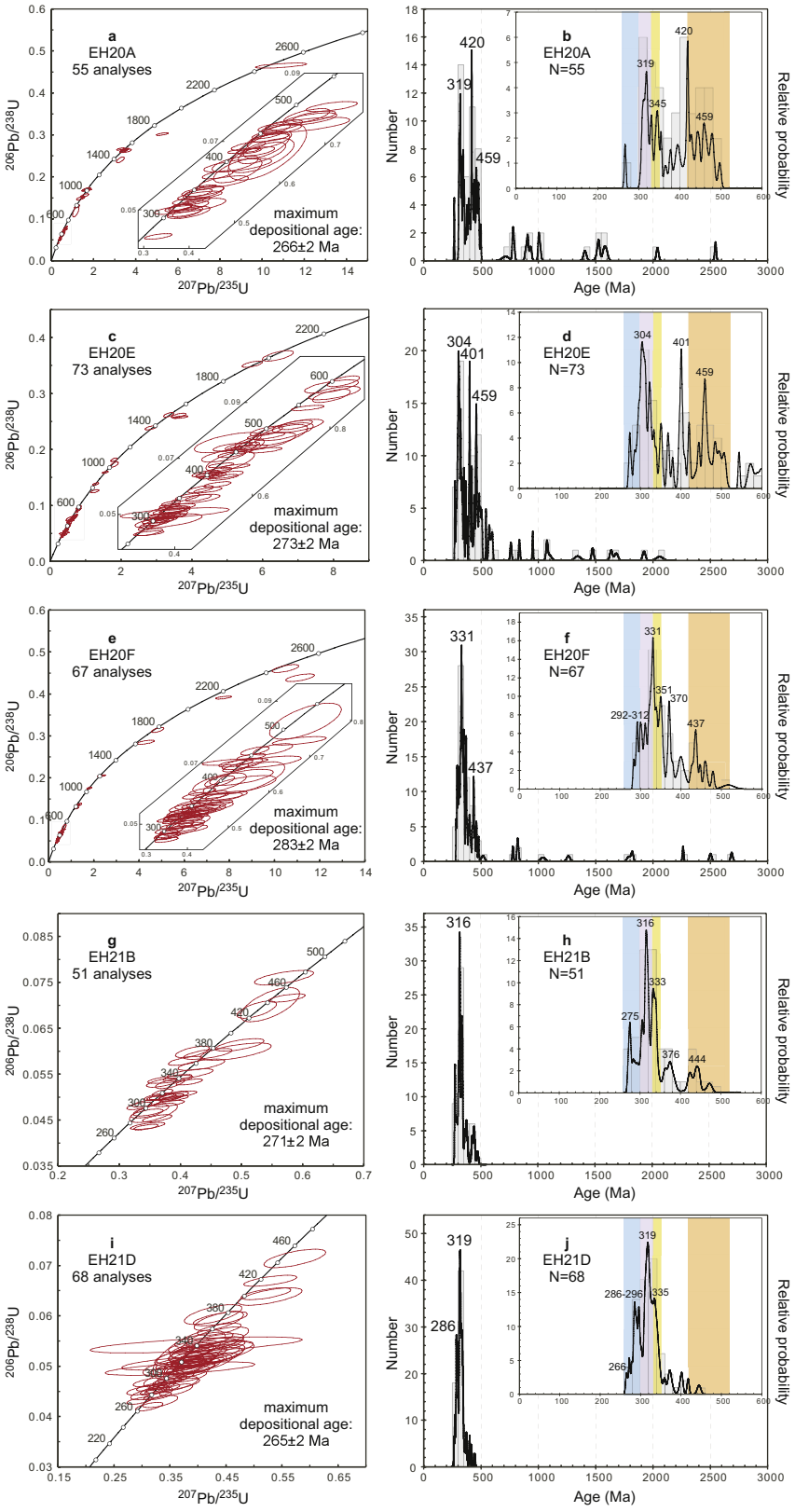

Figure 7. U-Pb concordia and probability diagrams of zircon ages for five rock samples from the Zhesi Formation.

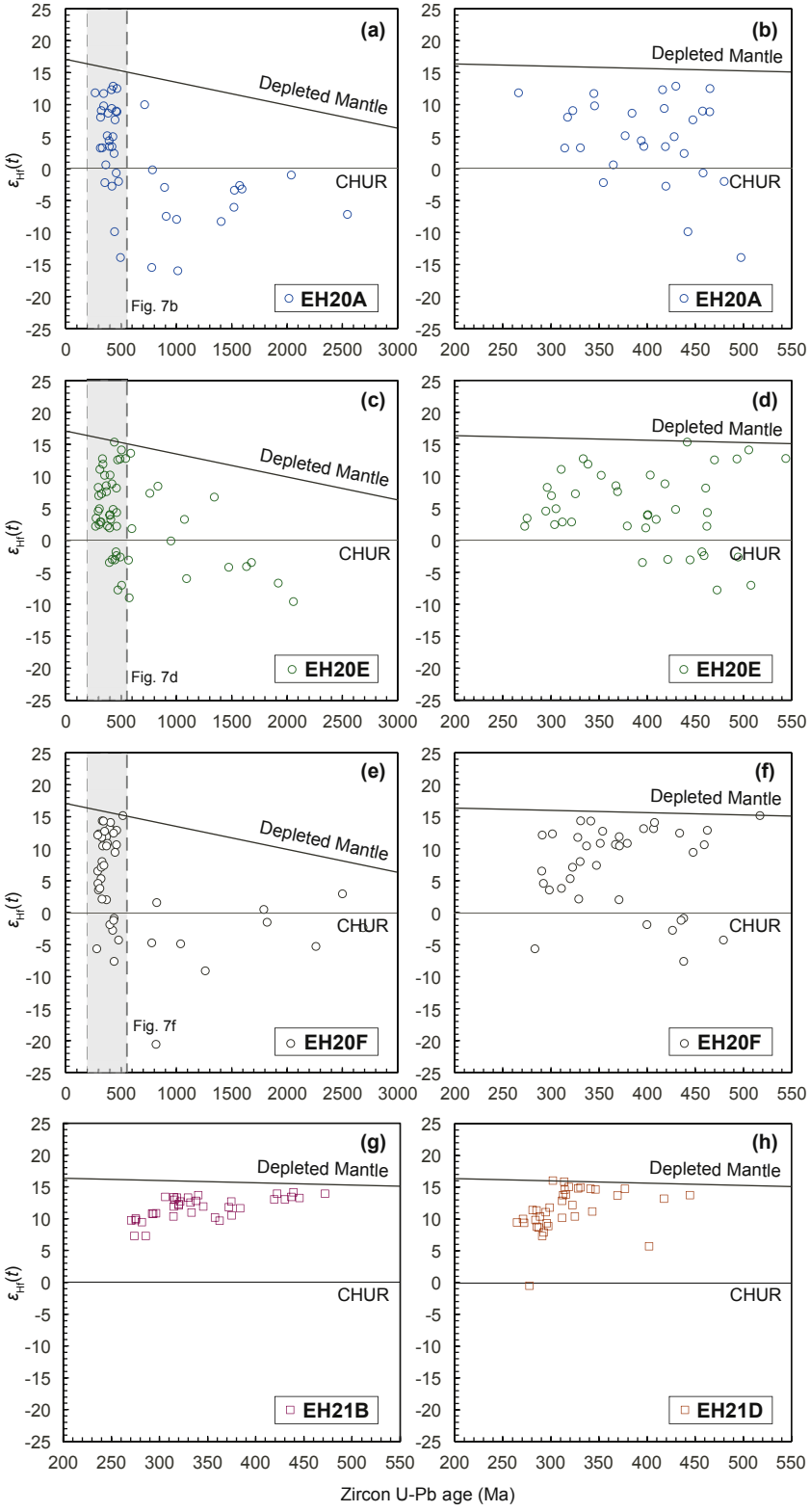

Figure 8. Plots of $\varepsilon_{Hf}(t)$ vs. U-Pb ages of detrital zircons from five rock samples collected from the Zhesi Formation. CHUR: Chondrite Uniform Reservoir.

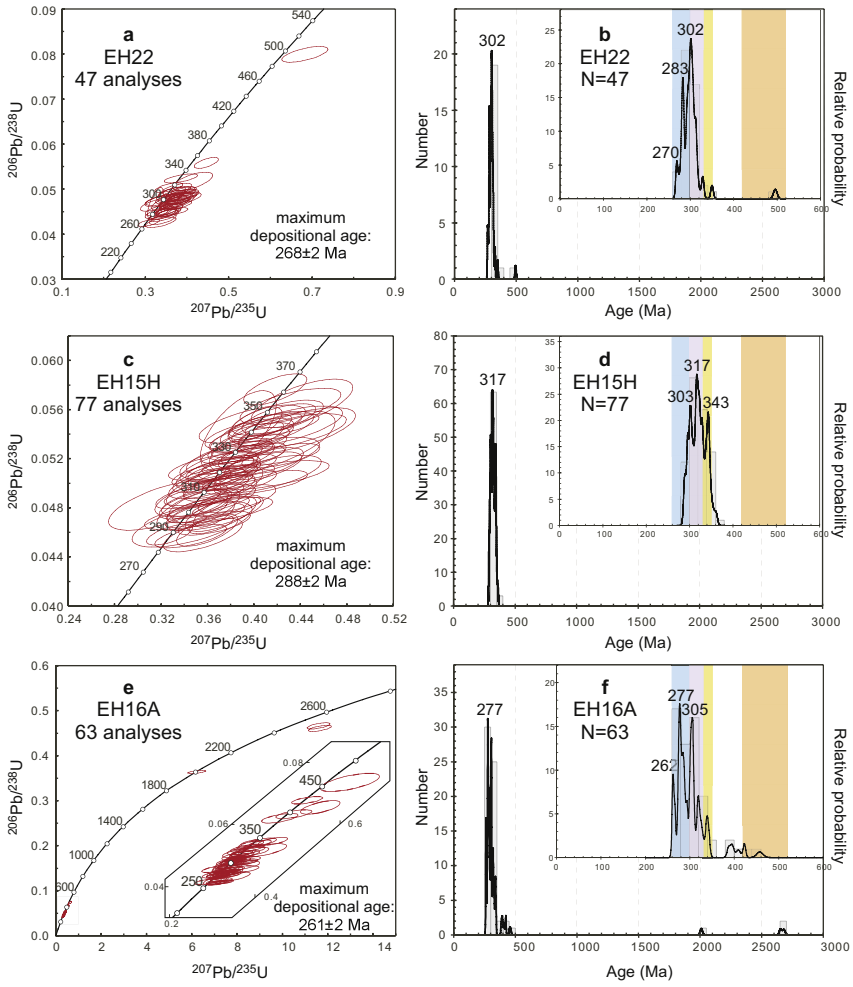

Figure 9. U-Pb concordia and probability diagrams of zircon ages of the remaining three rock samples (EH22, EH15H and EH16A) from the Bengbatu area.

the remaining three analyses give Precambrian ages, ranging from 2680 Ma to 2010 Ma. The youngest zircon yields a $^{206}Pb/^{238}U$ age of 261 ± 2 Ma, with discordance of <6%.

A total of 63 dated zircons from the above-stated two samples were analyzed for Hf isotopes. These zircons show highly variable $\varepsilon_{Hf}(t)$ values, ranging from −17.15 to +14.04 (Fig. 10b–d). Their initial $^{176}Hf/^{177}Hf$ ratios range from 0.281023 to 0.282957, corresponding to the depleted mantle two-stage Hf model ages (T_{DM2}) of 3669–466 Ma. Notably, almost all Paleozoic zircons show positive $\varepsilon_{Hf}(t)$ values of 0.14–14.04 except for two spots that have negative values (−3.08 for spot #8 in sample EH15H and −6.67 for spot #18 in sample EH16A) (Fig. 10b and d). The Precambrian zircons generally show negative $\varepsilon_{Hf}(t)$ values from −17.15 to −0.4 except for one zircon that has a positive $\varepsilon_{Hf}(t)$ value of 0.94 (Spot #4 in sample EH16A) (Fig. 10c). Among these Paleozoic zircons, the lowest $\varepsilon_{Hf}(t)$ value (−6.67) occurs in a relatively young zircon with a $^{236}Pb/^{238}U$ age of 423 Ma (Spot #18 in sample EH16A), corresponding to the lowest $^{176}Hf/^{177}Hf$ ratio of 0.282323 and the oldest Hf model age (T_{DM2}) of 1827 Ma (Appendix Table 2).

5. Discussion

5.1. Depositional ages and some redefinitions in the published geological map

Due to the lack of robust age constraints and the limitations of early dating techniques, some information in published geological maps remains uncertain or loosely constrained, particularly on the ages and structural relations of major lithological units. The large uncertainty hampers understanding of the overall tectonic evolution. As discussed below, our detrital zircon ages provide new constraints that allow some redefinitions of major lithological units and structures in published geological maps.

The strata that we studied in the south Yixigen area were previously presumed to deposit during Early Carboniferous time (IMBGMR, 1965, 1991). However, our results reveal that the youngest concordant zircons (discordance <6%) from the strata (samples EH15H and EH16A) give ages of ~288 Ma and ~261 Ma (Fig. 9c-f), and yield the youngest age peak at ~262 Ma (Fig. 9f). As a result, the age of 261 Ma represents the best estimate for the maximum depositional age, which is consistent with the youngest age peak at ~262 Ma in sample EH16A. This allows a redefinition of the deposition of the south Yixigen strata to be in the Middle Permian (Capitanian) or later, much younger than previously suspected. Such a redefinition requires the south Yixigen strata to have a fault or unconformity contact with the Carboniferous strata to the north, rather than the previously assumed depositional contact. Similarly, the strata that we studied in the north Yixigen area, previously thought to be deposited during Middle Devonian time (IMBGMR, 1965, 1991), have been redefined as the Middle Permian or younger strata, due to new recognitions of abundant Carboniferous–Permian zircons and the youngest zircon at ~268 Ma and the youngest age peak at ~270 Ma of detrital zircons from sample EH22 (Fig. 9a and b).

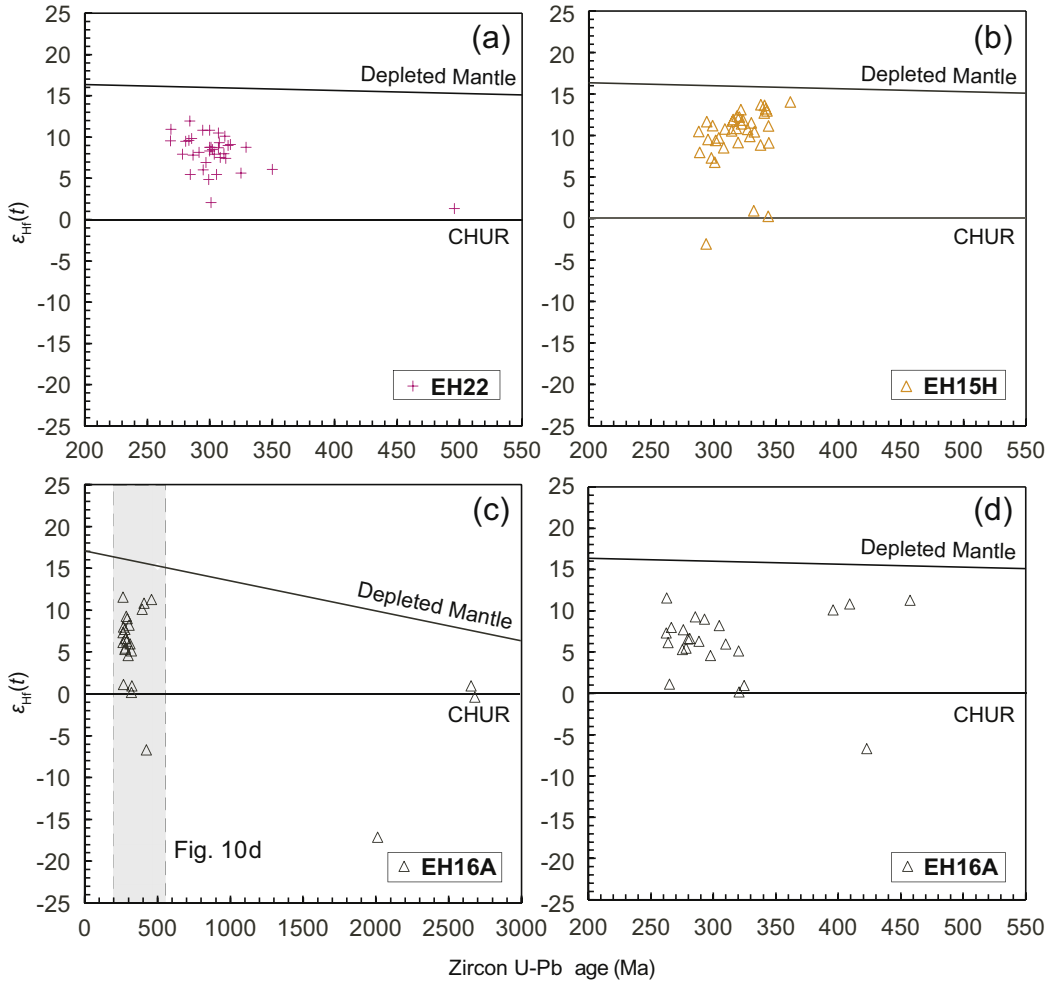

Figure 10. Plots of $\varepsilon_{Hf}(t)$ vs. U-Pb ages of detrital zircons from rock samples EH22, EH15H and EH16A. CHUR: Chondrite Uniform Reservoir.

The deposition of the Zhesi Formation was traditionally thought to have occurred during Early Permian time (IMBGMR, 1965, 1991). Wang et al. (2004) recognized conodont fauna from the Zhesi Formation and assigned an ambiguous Wordian to Capitanian age for its deposition. In this study, the youngest concordant zircons (discordance<10%) from five samples within the Zhesi Formation yield ages ranging from 283 Ma to 265 Ma (Fig. 7a–j), and the youngest age peak of detrital zircons from sample EH21D is ~266 Ma (Fig. 7j), both consistent with previous age determinations by Chen et al. (2015). These ages indicate that the Zhesi Formation was deposited at some time after ~265 Ma. Such an age determination is supported by the following two lines of evidence from the fossils and the sedimentary contact with age-constrained rock suites: (1) the recognition of conodont fauna from the Zhesi Formation allows assigning a Middle Permian age for its deposition (Wang et al., 2004); and (2) the Hegenshan ophiolite suites—unconformably overlain by the Zhesi Formation—were demonstrated to be emplaced before 280 Ma (Zhou et al., 2015), implying that the deposition of the Zhesi Formation must have postdated 280 Ma.

5.2. Provenances

Most detrital zircons from all samples exhibit oscillatory zoning and dominantly angular to sub-angular shape (Fig. 6), testifying to magmatic grains derived from near-source regions. Apart from several Precambrian grains that range from 2687 Ma to 544 Ma, three main Paleozoic age populations of detrital zircons have been commonly revealed: ca. 300–261 Ma, 351–300 Ma, and 517–419 Ma (Figs. 7, 9 and 11).

The 300-261 Ma detrital zircons are abundant and form a subordinate age population in the compilation of all dated zircons (Figs. 7, 9 and 11). Highly variable Hf isotopes (−5.68 to +12.12) of the zircons suggest that they were derived from mixed magmas related to reworking of ancient crust and mantle differentiation. Contemporaneous magmatic events, commonly associated with post-collisional orogenic collapse and crustal extension, occurred mainly in adjacent Mongolian arcs and the Northern Accretionary Orogen, including: (1) the 290–276 Ma calc-alkaline bimodal volcanic suites and peralkaline-alkaline A-type granites in the Mongolian arcs (Hong et al., 1994; Zhang et al., 2011, 2015b; Tong et al., 2015); (2) the ~284–274 Ma bimodal volcanic rocks (Zhang et al., 2008; Chen et al., 2014) and intrusive plutons (Bao et al., 2007a) in Xi Ujimqin Banner; and (3) the ~285–276 Ma Xilinhot A-type granites in the Northern Accretionary Orogen (Shi et al., 2004; Tong et al., 2015). Accordingly, it is possible that the 300–261 Ma detrital zircons were sourced from the Mongolian arcs and the Northern Accretionary Orogen.

The 351–300 Ma detrital zircons are most abundant in all dated samples (Figs. 6, 8 and 10). A conspicuous feature of these zircons is their highly positive $\varepsilon_{Hf}(t)$ values, implying that the parental magmas were differentiated from the depleted mantle. Synchronous arc-related magmas that resulted from the northward

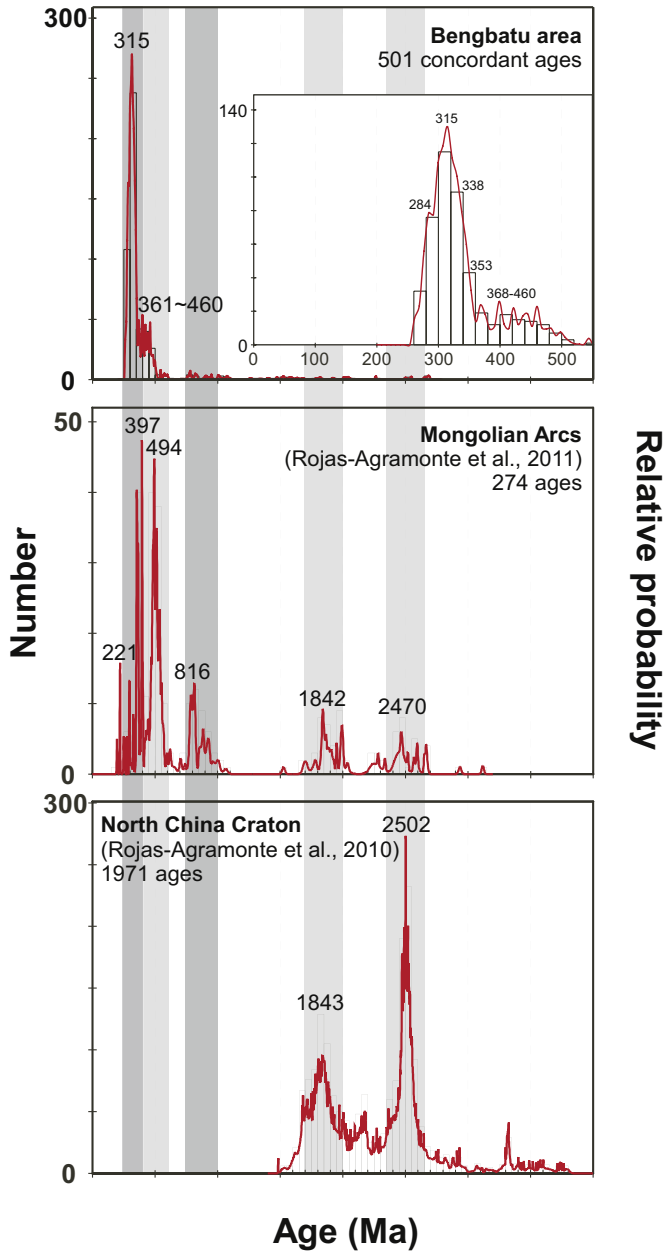

Figure 11. Comparison of age populations of the Permian sedimentary successions in the Bengbatu area with those of surrounding possible provenance terranes.

subduction of the Paleo-Asian Oceanic lithosphere have been widely documented in the Mongolian arcs and the Northern Accretionary Orogen, including: (1) the ~350–300 Ma calc-alkaline magmas (e.g., granodiorites, andesites, quartz monzonites, and quartz diorites) in South Mongolia (Kovalenko et al., 2006; Yarmolyuk et al., 2008; Blight et al., 2010; Wainwright et al., 2011); (2) the 350–340 Ma granitoids and gneissic granites in north of the Gobi-Altai Zone (Kröner et al., 2010); (3) the ~310 Ma gabbroic diorites and 322–316 Ma granitoids from the Balidao magma suite (Chen et al., 2000, 2009; Hu et al., 2015); and (4) the 330–313 Ma quartz diorites and granitoids in the Xilinhot area (Bao et al., 2007b; Liu et al., 2010a; Zhou, 2012). In addition, CL images in some 351–300 Ma zircons exhibit partially developed crystal faces or planar banded growth zones (Fig. 6), characterizing zircons crystallized from gabbroic rocks (Baines et al., 2009; Grimes et al., 2009; Koglin et al., 2009; Jian et al., 2012). Notably, gabbroic rocks are mainly distributed in the Erenhot-Hegenshan Ophiolite Belt, and recent SHRIMP and SIMS U-Pb zircon dating results yield ages of 356–346 Ma for their emplacement. Examples include: 354 ± 5 Ma and 353 ± 4 Ma for two gabbros from the eastern Erenhot ophiolite (Zhang et al., 2015c); 356 ± 5 Ma and 346 ± 2 Ma for two gabbros from the Xi-Ujimqi and Diyanmiao ophiolites (Song et al., 2015); and 354 ± 7 Ma for a gabbro from the Hegenshan ophiolite (Jian et al., 2012). As a result, we infer that the 351–300 Ma detrital zircons were derived from three major provenance terranes: (1) the Mongolian arcs; (2) the Erenhot-Hegenshan Ophiolite Belt; and (3) the Northern Accretionary Orogen.

The 517–419 Ma detrital zircons form another subordinate age population in all dated zircons (Figs. 7, 9 and 11). Highly variable Hf isotopes (−13.97 to +15.31) of the zircons reflect a source heterogeneity that implies a mixed origin of parental magmas, related to the melting of both ancient and juvenile crustal material. In the adjacent Northern Accretionary Orogen and the Mongolian arcs, early Paleozoic arc-related magmatic rocks that record the subduction of the Paleo-Asian Ocean, accretion and forearc generation are extensively distributed, including (1) the 498–418 Ma calc-alkaline plutons (e.g., plagiogranites, gabbros, tonalities, granodiorites, and quartz diorites) that constitute an early to mid-Paleozoic arc system in the Baiyanbaolidao area (Xu and Chen, 1997; Chen et al., 2000; Shi et al., 2003, 2005a, b; Zhang et al., 2004; Jian et al., 2008); (2) the ~421 Ma arc magmas and ~452–437 Ma migmatites in the Xilinhot area (Shi et al., 2003; Xue et al., 2009; Ge et al., 2011); (3) the 477–431 Ma alkaline to calc-alkaline magmas (e.g., orthogneisses, amphibolites and gneissic granites) in the Hutag Uul block (Yarmolyuk et al., 2005; Jian et al., 2010; Li et al., 2010); and (4) the ~502–411 Ma calc-alkaline magmas that constitute an island arc-forearc system in South Mongolia (Helo et al., 2006; Demoux et al., 2009; Kröner et al., 2010, 2011). Therefore, the Northern Accretionary Orogen and the Mongolian arcs were two potentially important sources for 517–419 Ma detrital zircons.

Less frequently Precambrian detrital zircons have been locally detected in Permian samples (Figs. 7, 9 and 11). To the south of the study area, despite extensive Precambrian rocks in North China (Zhao et al., 2006; Zhao and Cawood, 2012; Chen et al., 2017b), recent studies indicate that the intervening Paleo-Asian Ocean was not closed and prevented the detritus entering the study area during Middle Permian time (e.g., Eizenhöfer et al., 2015a, b), thus ruling out the possibility of the North China-derived contributors. Instead, the Mongolian arcs might be a significant provider of Precambrian detritus, by considering the voluminous Precambrian magmatism associated with assemblage and break-up of Rodinia therein (Wang et al., 2001; Demoux et al., 2009; Kröner et al., 2010, 2011; Rojas-Agramonte et al., 2011).

To sum up, possible source terranes that could have delivered clastic sediment to the Bengbatu area during Middle Permian time are the Mongolian arcs to the north, the Northern Accretionary Orogen to the south, and the intervening Erenhot-Hegenshan Ophiolite Belt.

5.3. Tectonic implications

In view of the above-stated provenance terranes, detrital zircons in the Bengbatu area contain wealthy information regarding episodic magmatism in the Mongolia arcs, the Northern Accretionary Orogen, and the Erenhot-Hegenshan Ophiolite Belt of southeastern CAOB. A compilation of Paleozoic detrital zircon Hf isotopes is presented in Fig. 12, and shows the following zircon $\varepsilon_{Hf}(t)$-time patterns: ca. 500–350 Ma and ca. 300–261 Ma zircons that are characterized by a large spread of $\varepsilon_{Hf}(t)$ values (−13.97 to +15.31), and ca. 350–300 Ma zircons that are dominated by

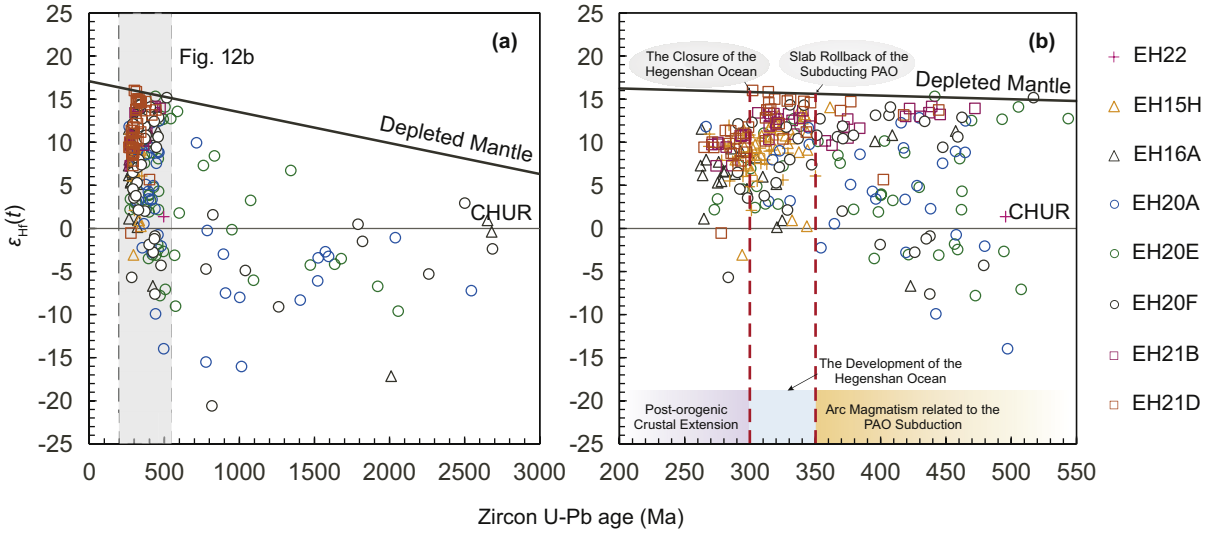

Figure 12. Plot of $\varepsilon_{Hf}(t)$ vs. U-Pb ages of detrital zircons for all studied rock samples from the Permian strata in the Bengbatu area. CHUR: Chondrite Uniform Reservoir.

positive $\varepsilon_{Hf}(t)$ values (+0.14 to +16.00). Two abrupt changes between mixed and positive $\varepsilon_{Hf}(t)$ values occur at ca. 350–330 Ma and ca. 300 Ma. As discussed below, the Hf isotope variations, combined with regional magmatic records, provide crucial constraints on the Paleozoic tectonic evolution of southeastern CAOB.

During Early Ordovician to Devonian time, the northward subduction of the Paleo-Asian oceanic lithosphere led to progressive accretion of the Northern Accretionary Orogen onto the Uliastai Continental Margin, forming a coherent terrane in southeastern CAOB (Fig. 13a). The melting of the mantle wedge, induced by hydrous fluids released during dehydration reactions in the subducting lithosphere (e.g., Defant and Drummond, 1990), produced voluminous ~490–417 Ma calc-alkaline arc magmatic rocks in the coherent terrane (e.g., Chen et al., 2000; Shi et al., 2003, 2005a, b; Jian et al., 2008, 2010; Kröner et al., 2010, 2011). Zircons from the magmatic rocks in this study display highly variable $\varepsilon_{Hf}(t)$ values of (−9.92 to +15.31) (Fig. 12), probably resulting from potential incorporation of supracrustal sedimentary components into magma sources during reworking of juvenile arc-derived crust.

During Early Carboniferous time, the Hegenshan Ocean was opened and separated the Northern Accretionary Orogen from the Uliastai Continental Margin (Xu et al., 2017; Fig. 13b). The ~350–335 Ma Eastern Erenhot and Hegenshan ophiolites (Zhang et al., 2015c; Zhou et al., 2015), as the remnants of the oceanic lithosphere, represent the best manifests of the assumed ocean opening. Our results reveal a significant shift from mixed to positive $\varepsilon_{Hf}(t)$ values at ca. 350–330 Ma (Fig. 12), possibly recording incipient opening of the ocean. We interpret the ocean opening as back-arc extension resulting from slab rollback of the subducting Paleo-Asian Oceanic lithosphere (Xu et al., 2017). This interpretation provides a causative mechanism for the significantly increased $\varepsilon_{Hf}(t)$ values (Fig. 12), as the back-arc extension generally involves more contribution of mantle-derived juvenile material to magma sources (e.g., Kemp et al., 2009; Collins et al., 2011). Accordingly, regional Carboniferous volcano-clastic rocks might represent sedimentary infills in a back-arc basin (Xu et al., 2017). During or soon after the ocean opening/spreading, the northward subduction of the Hegenshan Oceanic lithosphere beneath the Uliastai Continental Margin, as revealed by deep seismic reflection profiling (Zhang et al., 2014), might have occurred (Fig. 13b). This led to the generations of regional 350–310 Ma arc-related magmas to be related to the Hegenshan Ocean subduction, in addition to the Paleo-Asian Ocean subduction (Chen et al., 2000; Kovalenko et al., 2006; Yarmolyuk et al., 2008; Blight et al., 2010; Wainwright et al., 2011).

During Early Permian time, the final consumption of the Hegenshan Ocean led to the closure of the back-arc basin accompanied by the Hegenshan ophiolite emplacement (Zhou et al., 2015), which was responsible for amalgamation of the Northern Accretionary Orogen and the Uliastai Continental Margin along the Erenhot-Hegenshan Ophiolite Belt (Fig. 13c). Given that the Zhesi Formation and its equivalents unconformably overlie the Hegenshan ophiolites (Zhou et al., 2015), they might represent post-orogenic deposition that postdated the closure of the back-arc basin. This also gives plausible explanations for provenance determinations that the Bengbatu area received detritus from the Mongolian arcs to the north and the Northern Accretionary Orogen to the south during Middle Permian time. Notably, sedimentary rocks of the Zhesi Formation were bounded to the north by a normal fault (Fig. 3). This normal fault appears to dominate the crustal subsidence and sedimentary infilling of the Zhesi Formation, indicating an extensional tectonic setting for the deposition of the Zhesi Formation. The inferred crustal extension is further supported by regional-scale A-type and bimodal magmatism during Permian time (Shi et al., 2004; Bao et al., 2007a; Zhang et al., 2008; Zhou, 2012; Shao et al., 2014; Li et al., 2015). These A-type and bimodal magmatic rocks yield U-Pb zircon ages of 290–270 Ma, indicating that regional crustal extension might have commenced in the Early Permian (e.g., Zhang et al., 2011, 2015b; Shao et al., 2014; Tong et al., 2015). Accordingly, a significant tectonic switch from syn-orogenic subduction-related arc setting to post-orogenic extensional setting during Early Permian time might have existed. The switch is also manifested by the prominently decreased $\varepsilon_{Hf}(t)$ values at ca. 300–290 Ma (Fig. 12), which requires a greater crustal input into magma sources. Geodynamically, we interpret the extension as resulting from the post-orogenic collapse of the formerly overthickened crust possibly related to the Late Carboniferous closure of the back-arc basin.

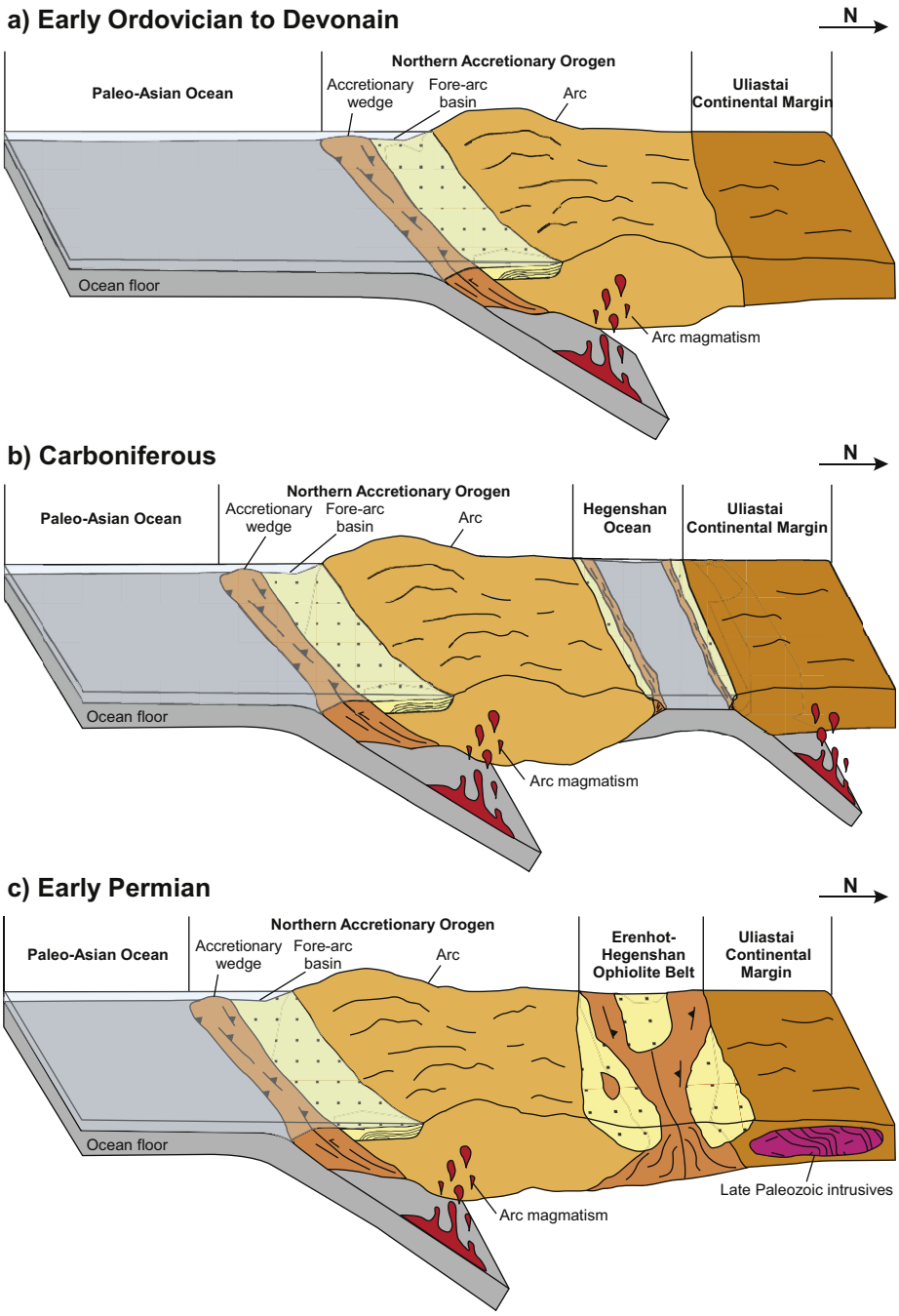

Figure 13. Schematic model for tectonic evolution of the southeastern CAOB during Ordovician to Early Permian time.

6. Conclusions

In situ zircon U-Pb and Hf-isotopic data have been determined for previously defined Devonian, Carboniferous and Early Permian strata in the Bengbatu area. Our results, combined with regional magmatic records, allow drawing the following main conclusions:

(1) Detrital zircons from these strata yield major age populations: ca. 300–261 Ma, 351–300 Ma, 517–419 Ma and 2687–544 Ma. Among them, the youngest ages redefine all these strata to have been deposited during Middle Permian (Wordian-Capitanian) time or later, much younger than previously considered.

(2) The possible detrital sources that could have delivered clastic sediments to the Bengbatu area in the Middle Permian are the Mongolian arcs to the north, the Northern Accretionary Orogen to the south, and the intervening Erenhot-Hegenshan Ophiolite Belt.

(3) Zircons with magmatic ages of ca. 500–350 Ma and ca. 300–260 Ma zircons display a large spread of $\varepsilon_{Hf}(t)$ values (−13.97 to +15.31), whereas ca. 350–300 Ma zircons are dominated by positive $\varepsilon_{Hf}(t)$ values (+0.14 to +16.00).

(4) Two abrupt changes between mixed and positive $\varepsilon_{Hf}(t)$ values occur at ca. 350–330 Ma and ca. 300 Ma. The former possibly manifests the incipient opening of the Hegenshan Ocean, due to slab rollback of the subducting Paleo-Asian Oceanic

lithosphere, whereas the latter likely corresponds to a major tectonic switch from syn-orogenic subduction-related to post-orogenic extensional setting, most likely related to extensional collapse of the formerly overthickened crust.

Acknowledgements

This research was financially supported by the National Natural Science Foundation of China (Grant Nos. 41730213, 41190075, 41190070), the Hong Kong Research Grants Council General Research Fund (17301915), and the HKU Seed Funding Programme for Basic Research (201611159210). This paper is a contribution to IGCP#648. We thank Prof. Xiaoming Liu and other staff of the State Key Laboratory of Continental Dynamics, Northwest University in Xi'an, China, for their kind help during zircon U-Pb and Hf analysis. We would also like to thank two anonymous reviewers for their constructive comments that helped us improve our paper.

Appendix A. Supplementary data

Supplementary data related to this article can be found at https://doi.org/10.1016/j.gsf.2018.08.003.

References

Badarch, G., Gunningham, W.D., Windley, B.F., 2002. A new terrane subdivision for Mongolia: implications for the Phanerozoic crustal growth of Central Asia. Journal of Asian Earth Sciences 21, 87–110.

Baines, A.G., Cheadle, M.J., John, B.E., Grimes, C.B., Schwartz, J.J., Wooden, J.L., 2009. SHRIMP Pb/U zircon ages constrain gabbroic crustal accretion at Atlantis Bank on the ultraslow-spreading Southwest Indian Ridge. Earth and Planetary Science Letters 287, 540–550.

Bao, Q.Z., Zhang, C.J., Wu, Z.L., Wang, H., Li, W., Sang, J.H., Liu, Y.S., 2007a. Zircon SHRIMP U–Pb dating of granitoids in a Late Paleozoic rift area, southeastern Inner Mongolia, and its implications. Geology in China 34, 790–798 (in Chinese with English abstract).

Bao, Q.Z., Zhang, C.J., Wu, Z.L., Wang, H., Li, W., Sang, J.H., Liu, Y.S., 2007b. SHRIMP U–Pb zircon geochronology of a Carboniferous quartz–diorite in Baiyingaole area, Inner Mongolia and its implications. Journal of Jilin University (Earth Science Edition) 37, 15–23 (in Chinese with English abstract).

Blight, J.H.S., Petterson, M.G., Crowley, Q.G., Cunningham, D., 2010. The Oyut Ulaan Volcanic group: stratigraphy, magmatic evolution and timing of Carboniferous arc development in Mongolia. Journal of the Geological Society 167, 491–509.

Bouvier, A., Vervoort, J.D., Patchett, P.J., 2008. The Lu-Hf and Sm-Nd isotopic composition of CHUR: constraints from unequilibrated chondrites and implications for the bulk composition of terrestrial planets. Earth and Planetary Science Letters 273, 48–57.

Briggs, S.M., Yin, A., Manning, C.E., Chen, Z.L., Wang, X.F., Grove, M., 2007. Late paleozoic tectonic history of the ertix fault in the Chinese altai and its implications for the development of the central asian orogenic system. The Geological Society of America Bulletin 119, 944–960.

Cawood, P.A., Hawkesworth, C.J., Dhuime, B., 2012. Detrital zircon record and tectonic setting. Geology 40 (10), 875–878.

Chen, B., Jahn, B.M., Wilde, S., Xu, B., 2000. Two contrasting Paleozoic magmatic belts in northern Inner Mongolia, China: petrogenesis and tectonic implications. Tectonophysics 328, 157–182.

Chen, B., Jahn, B.M., Tian, W., 2009. Evolution of the Solonker suture zone: constraints from zircon U-Pb ages, Hf isotopic ratios and whole-rock Nd–Sr isotope compositions of subduction and collision-related magmas and forearc sediments. Journal of Asian Earth Sciences 34, 245–257.

Chen, N.H.C., Zhao, G.C., Jahn, B.M., Zhou, H., Sun, M., 2017a. Geochemistry and geochronology of the delinggou intrusion: implications for the subduction of the Paleo-Asian ocean beneath the north China craton. Gondwana Research 43, 178–192.

Chen, N.H.C., Zhao, G.C., Jahn, B.M., Sun, M., Zhou, H., 2017b. U-Pb zircon ages and Hf isotopes of ~2.5 Ga granitoids from the Yinshan Block, North China Craton: implications for crustal growth. Precambrian Research 303, 171–182.

Chen, Y., Zhang, Z.C., Li, K., Luo, Z.W., Tang, W.H., Li, Q.G., 2014. Geochronology, geochemistry and geological significance of the Permian bimodal volcanic rocks in Xi Ujimqin Banner, Inner Mongolia. Acta Scientiarum Naturalium Universitatis Pekinensis 50, 843–858 (in Chinese with English abstract).

Chen, Y., Zhang, Z.C., Li, K., Li, Q.G., Luo, Z.W., 2015. Provenance of the Middle Permian Zhesi Formation in central Inner Mongolia, northern China: constraints from petrography, geochemistry and detrital zircon U–Pb geochronology. Geological Journal 36 (4), 274–297.

Collins, W.J., Belousova, E.A., Kemp, A.I.S., Murphy, J.B., 2011. Two contrasting Phanerozoic orogenic systems revealed by hafnium isotope data. Nature Geoscience 4, 333–337.

Daoudene, Y., Gapais, D., Ruffet, G., Gloaguen, E., Cocherie, A., Ledru, P., 2012. Synthinning pluton emplacement during Mesozoic extension in eastern Mongolia. Tectonics 31 (3), 160–164.

Defant, M.J., Drummond, M.S., 1990. Derivation of some modern arc magmas by melting of young subducted lithosphere. Nature 347, 662–665.

Demoux, A., Kröner, A., Liu, D., Badarch, G., 2009. Precambrian crystalline basement in southern Mongolia as revealed by SHRIMP zircon dating. International Journal of Earth Sciences 98, 1365–1380.

Diwu, C.R., Sun, Y., Zhang, H., Wang, Q., Guo, A.L., Fan, L.G., 2012. Episodic tectonothermal events of the western North China Craton and North Qinling Orogenic Belt in central China: constraints from detrital zircon U-Pb ages. Journal of Asian Earth Sciences 47, 107–122.

Eizenhöfer, P.R., Zhao, G.C., Zhang, J., Sun, M., 2014. Final closure of the Paleo-Asian ocean along the solonker suture zone: constraints from geochronological and geochemical data of permian volcanic and sedimentary rocks. Tectonics 33, 441–463.

Eizenhöfer, P.R., Zhao, G.C., Sun, M., Zhang, J., Han, Y.G., Hou, H., 2015a. Geochronological and Hf isotopic variability of detrital zircons in Palaeozoic sedimentary strata across the accretionary collision Zone between the North China Craton and the Mongolian arcs, and its tectonic implications. The Geological Society of America Bulletin 127, 1422–1436.

Eizenhöfer, P.R., Zhao, G.C., Zhang, J., Han, Y.G., Hou, W.Z., Liu, D.X., Wang, B., 2015b. Geochemical characteristics of the Permian basins and their provenances across the Solonker Suture Zone: assessment of net crustal growth during the closure of the Palaeo-Asian Ocean. Lithos 224–225, 240–255.

Fedorovskii, V.S., Khain, E.E., Vladimirov, A.G., Kargopolov, S.A., Gibsher, A.S., Izokh, A.E., 1995. Tectonics, metamorphism, and magmatism of collisional zones of the Central Asian Caledonides. Geotectonics 29, 193–212.

Ge, M.C., Zhou, W.X., Yu, Y., Sun, J.J., Bao, J.Q., Wang, S.H., 2011. Dissolution and supracrustal rocks dating of Xilin gol complex, Inner Mongolia, China. Earth Science Frontiers 18 (5), 182–195 (in Chinese with English abstract).

Griffin, W.L., Belousova, E.A., Shee, S.R., Pearson, N.J., O'reilly, S.Y., 2004. Archean crustal evolution in the northern Yilgarn Craton: U-Pb and Hf-isotope evidence from detrital zircons. Precambrian Research 131, 231–282.

Grimes, C.B., John, B.E., Cheadle, M.J., Mazdab, F.K., Wooden, J.L., Swapp, S., Schwartz, J.J., 2009. On the occurrence, trace element geochemistry, and crystallization history of zircon from in situ ocean lithosphere. Contributions to Mineralogy and Petrology 158, 757–783.

Han, Y.G., Zhao, G.C., Sun, M., Eizenhöfer, P.R., Hou, W.Z., Zhang, X.R., Liu, D.X., Wang, B., Zhang, G.W., 2015. Paleozoic accretionary orogenesis in the Paleo-Asian Ocean: insights from detrital zircons from Silurian to Carboniferous strata at the northwestern margin of the TarimCraton. Tectonics 34, 334–351.

Han, Y.G., Zhao, G.C., Cawood, P.A., Sun, M., Eizenhöfer, P.R., Hou, W.Z., Zhang, X.R., Liu, Q., 2016a. Tarim and North China cratons linked to northern Gondwana through switching accretionary tectonics and collisional orogenesis. Geology 44, 95–98.

Han, Y.G., Zhao, G.C., Sun, M., Eizenhöfer, P.R., Hou, W.Z., Zhang, X.R., Liu, Q., Wang, B., Liu, D.X., Xu, B., 2016b. Late paleozoic subduction and collision processes during the amalgamation of the central asian orogenic belt along the south tianshan suture zone. Lithos 246–247, 1–12.

Helo, C., Hegner, E., Kroner, A., Badarch, G., Tomurtogoo, O., Windley, B.F., Dulski, P., 2006. Geochemical signature of Paleozoic accretionary complexes of the central Asian Orogenic Belt in South Mongolia: constraints on arc environments and crustal growth. Chemical Geology 227, 236–257.

Heubeck, C., 2001. Assembly of central Asia during the middle and late Paleozoic. In: Hendrix, M.S., Davis, G.A. (Eds.), Paleozoic and Mesozoic Tectonic Evolution of Central and Eastern Asia: From Continental Assembly to Intracontinental Deformation, vol. 194. Geological Society of American Memoir, pp. 1–22.

Hong, D.W., Huang, H.Z., Xiao, Y.J., Xu, H.M., 1994. The Permian alkaline granites in central Inner Mongolia and their geodynamic significance. Acta Geologica Sinica 68 (3), 219–230.

Hsü, K.J., Wang, Q.C., Li, L., Hao, J., 1991. Geological evolution of the Neimonides: a working hypothesis. Eclogae Geologicae Helvetiae 84 (1), 1–31.

Hu, C.S., Li, W.B., Xu, C., Zhong, R., Zhu, F., 2015. Geochemistry and zircon U-Pb-Hf isotopes of the granitoids of Baolidao and Halatu plutons in Sonidzuoqi area, Inner Mongolia: implications for petrogenesis and geodynamic setting. Journal of Asian Earth Sciences 97, 294–306.

IMBGMR (Inner Mongolian Bureau of Geology and Mineral Resources), 1965. 1:200,000 Scale Geological Map of Bengbatu. Geological Map of P.R.C. Geological Publishing House, Beijing (in Chinese).

IMBGMR (Inner Mongolian Bureau of Geology and Mineral Resources), 1991. Regional Geology of Inner Mongolian Autonomous Region. Geological Publishing House, Beijing (in Chinese with English abstract).

Jackson, S.E., Pearson, N.J., Griffin, W.L., Belousova, E.A., 2004. The application of laser ablation-inductively coupled plasma-mass spectrometry to in situ U-Pb zircon geochronology. Chemical Geology 211 (1–2), 47–69.

Jian, P., Liu, D.Y., Kröner, A., Windley, B.F., Shi, Y.R., Zhang, F.Q., Shi, G.H., Miao, L.C., Zhang, W., Zhang, Q., Zhang, L.Q., Ren, J.S., 2008. Time scale of an early to mid-Paleozoic orogenic cycle of the long-lived Central Asian Orogenic Belt, Inner Mongolia of China: implications for continental growth. Lithos 101, 233–259.

Jian, P., Liu, D., Kröner, A., Windley, B.F., Shi, Y., Zhang, W., Zhang, F., Miao, L., Zhang, L., Tomurhuu, D., 2010. Evolution of a permian intraoceanic arc-trench system in the solonker suture zone, central asian orogenic belt, China and Mongolia. Lithos 118, 169–190.

Jian, P., Kröner, A., Windley, B.F., Yuruo Shi, Y.R., Zhang, W., Zhang, L.Q., Yange, W.R., 2012. Carboniferous and Cretaceous mafic–ultramafic massifs in Inner Mongolia (China): a SHRIMP zircon and geochemical study of the previously presumed integral "Hegenshan ophiolite". Lithos 142–143, 48–66.

Kelty, T.K., Yin, A., Dash, B., Gehrels, G.E., Ribeiro, A.E., 2008. Detrital-zircon geochronology of paleozoic sedimentary rocks in the hangay-hentey basin, north-central Mongolia: implications for the tectonic evolution of the mongol-okhotsk ocean in central Asia. Tectonophysics 451, 290–311.

Kemp, A.I.S., Hawkesworth, C.J., Collins, W.J., Gray, C.M., Blevin, P.L., EIMF, 2009. Isotopic evidence for rapid continental growth in an extensional accretionary orogen: the Tasmanides, eastern Australia. Earth and Planetary Science Letters 284, 455–466.

Koglin, N., Kostopoulos, D., Reischmann, T., 2009. The Lesvos mafic–ultramafic complex, Greece: ophiolite or incipient rift? Lithos 108, 243–261.

Kovalenko, V.I., Yarmoluyk, V.V., Sal'nikova, E.B., Kozlovsky, A.M., Kotov, A.B., Kovach, V.P., Savatenkov, V.M., Vladykin, N.V., Ponomarchuk, V.A., 2006. Geology, geochronology and geodynamics of the Khan Bogd alkali granite pluton in southern Mongolia. Geotectonics 40, 450–466.

Kröner, A., Lehmann, J., Schulmann, K., Demoux, A., Lexa, O., Tomurhuu, D., Stipska, P., Liu, D., Wingate, M.T.D., 2010. Lithostratigraphic and geochronological constraints on the evolution of the central Asian Orogenic Belt in SW Mongolia: early Paleozoic rifting followed by late Paleozoic accretion. American Journal of Science 310, 523–574.

Kröner, A., Demoux, A., Zack, T., Rojas-Agramonte, Y., Jian, P., Tomurhuu, D., Barth, M., 2011. Zircon ages for a felsic volcanic rock and arc-related early Paleozoic sediments on the margin of the Baydrag microcontinent, central Asian orogenic belt, Mongolia. Journal of Asian Earth Sciences 42, 1008–1017.

Li, J.Y., 2006. Permian geodynamic setting of Northeast China and adjacent regions: closure of the Paleo-Asian Ocean and subduction of the Paleo-Pacific Plate. Journal of Asian Earth Sciences 26, 207–224.

Li, K., Zhang, Z.C., Feng, Z.S., Li, J.F., Tang, W.H., Luo, Z.W., Chen, Y., 2015. Two-phase magmatic events during late paleozoic in the North of the central Inner Mongolia-Da hinggan orogenic belt and its tectonic significance. Acta Geologica Sinica 89, 272–288 (in Chinese with English abstract).

Li, W.G., Li, Q.F., Jiang, W.D., 1996. Multiple Classification and Correlation of the Stratigraphy of China (15): Stratigraphy (Lithostratic) of Nei Mongol Autonomous Region. China University of Geosciences Press, Wuhan (in Chinese).

Li, X.H., Long, W.G., Li, Q.L., Liu, Y., Zheng, Y.F., Yang, Y.H., Chamberlain, K.R., Wan, D.F., Guo, C.H., Wang, X.C., 2010. Penglai zircon megacrysts: a potential new working reference material for microbeam determination of Hf–O isotopes and U–Pb age. Geostandards and Geoanalytical Research 34, 117–134.

Li, Y.L., Zhou, H.W., Brouwer, F.M., Wijbrans, J.R., Zhong, Z.Q., Liu, H.F., 2011. Tectonic significance of the Xilin Gol complex, Inner Mongolia, China: petrological, geochemical and U-Pb zircon age constraints. Journal of Asian Earth Sciences 42, 1018–1029.

Liu, X.M., Gao, S., Diwu, C.R., Ling, W.L., 2008. Precambrian crustal growth of Yangtze Craton as revealed by detrital zircon studies. American Journal of Science 308 (4), 421–468.

Liu, Y.F., Jiang, S.H., Zhang, Y., 2010a. The SHRIMP zircon U-Pb dating and geological features of Bairendaba diorite in the Xilin-haote area, Inner Mongolia, China. Geological Bulletin of China 29 (5), 688–696 (in Chinese with English abstract).

Liu, Y.S., Hu, Z.C., Zong, K.Q., Gao, C.G., Gao, S., Xu, J., Chen, H.H., 2010b. Reappraisement and refinement of zircon U–Pb isotope and trace element analyses by LA-ICP-MS. Chinese Science Bulletin 55 (15), 1535–1546.

Ludwig, K.R., 2003. A Geochronological Toolkit for Microsoft Excel, vol. 4. Berkeley Geochronology Center: Special Publication, pp. 25–32.

Meng, Q.R., 2003. What drove late Mesozoic extension of the northern China–Mongolia tract? Tectonophysics 369, 155–174.

Miao, L., Zhang, F., Fan, W., Liu, D., 2007. Phanerozoic evolution of the Inner Mongolia–Daxinganling Orogenic Belt in North China: constraints from geochronology of ophiolites and associated formations. In: Zhai, M.G., Windley, B.F., Kusky, T.M., Meng, Q.R. (Eds.), Mesozoic Sub-continental Lithospheric Thinning under Eastern Asia, vol. 280. Geological Society, London, Special Publications, pp. 223–237.

Miao, L.C., Fan, W.M., Liu, D.Y., Zhang, F.Q., Shi, Y.R., Guo, F., 2008. Geochronology and geochemistry of the Hegenshan ophiolitic complex: implications for late-stage tectonic evolution of the Inner Mongolia–Daxinganling orogenic belt, China. Journal of Asian Earth Sciences 32, 348–370.

Mossakovsky, A.A., Ruzhentsev, S.V., Samygin, S.G., Kheraskova, T.N., 1993. Central Asian fold belt: geodynamic evolution and history of formation. Geotectonics 6, 3–33.

Nie, F., Bjørlykke, A., 1999. Nd and Sr isotope constraints on the age and origin of Proterozoic meta-mafic volcanic rocks in the Bainaimiao-Wenduermiao district, south-central Inner Mongolia, China. Continental Dynamics 4, 1–14.

Robinson, P.T., Zhou, M.F., Hu, X.F., Reynolds, P., Bai, W., Yang, J., 1995. Geochemical constraints on petrogenesis and crustal accretion of the Hegenshan ophiolite, northern China. Acta Petrologica Sinica 11, 112–124 (in Chinese with English abstract).

Robinson, P.T., Zhou, M.F., Hu, X.F., Reynolds, P., Wenji, B., Yang, J.S., 1999. Geochemical constraints on the origin of the Hegenshan ophiolite, Inner Mongolia, China. Journal of Asian Earth Sciences 17, 423–442.

Rojas-Agramonte, Y., Kröner, A., Demoux, A., Xia, X., Wang, W., Donskaya, T., Liu, D., Sun, M., 2011. Detrital and xenocrystic zircon ages fromNeoproterozoic to palaeozoic arc terranes of Mongolia: significance for the origin of crustal fragments in the central Asian Orogenic Belt. Gondwana Research 19, 751–763.

Sengör, A.M.C., Natal'in, B.A., Burtman, V.S., 1993. Evolution of the Altaid tectonic collage and Paleozoic crustal growth in Eurasia. Nature 364 (6435), 299–307.

Sengör, A.M.C., Natal'in, B.A., 1996a. Paleotectonics of Asia: fragments of a synthesis. In: Yin, A., Harrison, M. (Eds.), The Tectonic Evolution of Asia. Cambridge University Press, Cambridge, pp. 486–641.

Sengör, A.M.C., Natal'in, B.A., 1996b. Turkic-type orogeny and its role in the making of the continental crust. Annual Review of Earth and Planetary Sciences 24, 263–337.

Shao, J.A., 1989. Continental crust accretion and tectono-magmatic activity at the northern margin of the Sino-Korean plate. Journal of Southeast Asian Earth Sciences 3, 57–62.

Shao, J.A., 1991. Crustal Evolution in the Middle Part of the Northern Margin of the Sino-Korean Plate. Peking University Publishing House, Beijing, China (in Chinese with English abstract).

Shao, J.A., Tang, K.D., He, G.Q., 2014. Early permian tectono-palaeogeographic reconstruction of Inner Mongolia, China. Acta Petrolei Sinica 30, 1858–1866 (in Chinese with English abstract).

Shen, S.Z., Zhang, H., Shang, Q.H., Li, W.Z., 2006. Permian stratigraphy and correlation of Northeast China: a review. Journal of Asian Earth Sciences 26 (3–4), 304–326.

Shi, G.H., Liu, D.Y., Zhang, F.Q., Jian, P., Miao, L.C., Shi, Y.R., Tao, H., 2003. SHRIMP U–Pb zircon geochronology of Xilin gol complex, Inner Mongolia, China, and its implications. Chinese Science Bulletin 48, 2742–2748.

Shi, G.H., Miao, L.C., Zhang, F.Q., Jian, P., Fan, W.M., Liu, D.Y., 2004. Emplacement age and tectonic implications of the Xilinhot A-type granite in Inner Mongolia, China. Chinese Science Bulletin 49, 723–729.

Shi, Y.R., Liu, D.Y., Zhang, Q., Jian, P., Zhang, F.Q., Miao, L.C., Shi, G.H., Zhang, L.Q., Tao, H., 2005a. The petrogenesis and SHRIMP dating of the Baiyinbaolidao adakitic rocks in south Suzuqi, Inner Mongolia. Acta Petrologica Sinica 21, 143–150 (in Chinese with English abstract).

Shi, Y.R., Liu, D.Y., Jian, P., Zhang, Q., Zhang, F.Q., Miao, L.C., Shi, G.H., Zhang, L.Q., Tao, H., 2005b. Zircon SHRIMP dating of krich granites in sonid zuoqi. Geological Bulletin of China 21, 424–428 (in Chinese with English abstract).

Song, S.G., Wang, M.M., Xu, X., Wang, C., Niu, Y.L., Allen, M.B., Su, L., 2015. Ophiolites in the Xing'an-Inner Mongolia accretionary belt of the CAOB: implications for two cycles of seafloor spreading and accretionary orogenic events. Tectonics 34 (10), 2221–2248.

Söderlund, U., Patchett, P.J., Vervoort, J.D., Isachsen, C.E., 2004. The ^{176}Lu decay constant determined by Lu-Hf and U-Pb isotope systematics of Precambrian mafic intrusions. Earth and Planetary Science Letters 219, 311–324.

Tang, K.D., 1990. Tectonic development of Paleozoic foldbelts at the northern margin of the Sino-Korean Craton. Tectonics 9, 249–260.

Tang, K.D., Yan, Z.Y., 1993. Regional metamorphism and tectonic evolution of the Inner Mongolian suture zone. Journal of Metamorphic Geology 11, 511–522.

Tong, Y., Jahn, B.M., Wang, T., Hong, D.W., Smith, E.I., Sun, M., Gao, J.F., Yang, Q.D., Huang, W., 2015. Permian alkaline granites in the Erenhot–Hegenshan belt, northern Inner Mongolia, China: model of generation, time of emplacement and regional tectonic significance. Journal of Asian Earth Sciences 97, 320–336.

Torsvik, T.H., Cocks, R.M., 2004. Earth geography from 400 to 250Ma: a paleomagnetic, faunal and facies review. Journal of the Geological Society 161, 555–572.

Wainwright, A.J., Tosdal, R.M., Wooden, J.L., Mazdab, F.K., Friedman, R.M., 2011. U-Pb (zircon) and geochemical constraints on the age, origin, and evolution of Paleozoic arc magmas in the Oyu Tolgoi porphyry Cu-Au district, southern Mongolia. Gondwana Research 19, 764–787.

Wang, C.Y., Wang, P., Li, W.G., 2004. Conodonts from the permian jisu honguer (Zhesi) formation of Inner Mongolia, China. Geobios 37, 471–480.

Wang, Q., Liu, X.Y., 1986. Paleoplate tectonics between cathaysia and angaraland in Inner Mongolia of China. Tectonics 5, 1073–1088.

Wang, T., Zheng, Y.D., Gehrels, G.E., Mu, Z.G., 2001. Geochronological evidence for existence of the south Mongolian microcontinent: a zircon U–Pb age of granitoid gneisses from the Yagan–Onch Hayrhan metamorphic core complex on the Sino–Mongolian border. China Science Bulletin 46, 2005–2008.

Wang, T., Zheng, Y.D., Zhang, J.J., Zeng, L.S., Donskaya, T., Guo, L., Li, J.B., 2011. Pattern and kinematic polarity of late Mesozoic extension in continental NE Asia: perspectives from metamorphic core complexes. Tectonics 30 (6), TC6007.

Windley, B.F., Alexeiev, D., Xiao, W.J., Kröner, A., Badarch, G., 2007. Tectonic models for accretion of the central asian orogenic belt. Journal of the Geological Society 164, 31–47.

Wu, F.Y., Yang, Y.H., Xie, L.W., Yang, J.H., Xu, P., 2006. Hf isotopic compositions of the standard zircons and baddeleyites used in U-Pb geochronology. Chemical Geology 234, 105–126.

Xiao, W.J., Windley, B.F., Hao, J., Zhai, M.G., 2003. Accretion leading to collision and the Permian Solonker suture, Inner Mongolia, China: termination of the central Asian orogenic belt. Tectonics 22 (6), 1069.

Xiao, W.J., Zhang, L.C., Qin, K.Z., Sun, S., Li, J.L., 2004. Paleozoic accretionary and collisional tectonics of the Eastern Tianshan (China): implications for the continental growth of central Asia. American Journal of Science 304, 370–395.

Xiao, W.J., Kröner, A., Windley, B., 2009a. Geodynamic evolution of central Asia in the paleozoic and mesozoic. International Journal of Earth Sciences 98, 1185–1188.

Xiao, W.J., Windley, B., Huang, B., Han, C., Yuan, C., Chen, H., Sun, M., Sun, S., Li, J., 2009b. End-Permian to mid-Triassic termination of the accretionary processes of the southern Altaids: implications for the geodynamic evolution, Phanerozoic continental growth, and metallogeny of Central Asia. International Journal of Earth Sciences 98, 1189–1217.

Xiao, W.J., Huang, B.C., Han, C.M., Sun, S., Li, J.L., 2010. A review of the western part of the Altaids: a key to understanding the architecture of accretionary orogens. Gondwana Research 18, 253–273.

Xiao, W.J., Windley, B.F., Allen, M.B., Han, C., 2013. Paleozoic multiple accretionary and collisional tectonics of the Chinese Tianshan orogenic collage. Gondwana Research 23, 1316–1341.

Xiao, W.J., Windley, B.F., Sun, S., Li, J.L., Huang, B.C., Han, C.M., Yuan, C., Sun, M., Chen, H.L., 2015. A tale of amalgamation of three permo-triassic collage systems in central Asia: oroclines, sutures, and terminal accretion. Annual Review of Earth and Planetary Sciences 43, 16.1–16.31.

Xiao, W.J., Santosh, M., 2014. The western Central Asian Orogenic Belt: a window to accretionary orogenesis and continental growth. Gondwana Research 25, 1429–1444.

Xu, B., Chen, B., 1997. Framework and evolution of the middle Paleozoic orogenic belt between Siberian and North China plates in northern Inner Mongolia. Science in China Series D-Earth Sciences 40, 463–469 (in Chinese).

Xu, B., Charvet, J., Chen, Y., Zhao, P., Shi, G.Z., 2013. Middle Paleozoic convergent orogenic belts in western Inner Mongolia (China): framework, kinematics, geochronology and implications for tectonic evolution of the Central Asian Orogenic Belt. Gondwana Research 23, 1342–1364.

Xu, B., Zhao, G.C., Li, J.H., Liu, D.X., Wang, B., Han, Y.G., Eizenhöfer, P.R., Zhang, X.R., Hou, W.Z., Liu, Q., 2017. Ages and Hf isotopes of detrital zircons from paleozoic strata in the chagan obo temple area, Inner Mongolia: implications for the evolution of the central asian orogenic belt. Gondwana Research 43, 149–163.

Xue, H.M., Guo, L.J., Hou, Z.Q., Zhou, X.W., Tong, Y., Pan, X.F., 2009. The Xilingele complex from the eastern part of the Central Asian–Mongolia Orogenic Belt, China: products of of Early Variscan orogeny other than ancient block: evidence from zircon SHRIMP U–Pb ages. Acta Petrologica Sinica 25 (8), 2001–2010 (in Chinese with English abstract).

Yakubchuk, A., 2004. Architecture and mineral deposit set- tings of the Altaid orogenic collage: a revised model. Journal of Asian Earth Sciences 23, 761–779.

Yang, Z.Y., Liu, H., Zhang, D.J., Li, X., Sun, Y.W., 2015. Detrital zircon U–Pb dating of upper carboniferous–lower permian Amushan Formation in bayan obo area, Inner Mongolia and its geological implications. Global Geology 34, 259–272 (in Chinese with English abstract).

Yarmolyuk, V.V., Kovalenko, V.I., Sal'nikova, E.B., Kozakov, I.K., Kotov, A.B., Kovach, V.P., Vladykin, N.V., Yakovleva, S.Z., 2005. U–Pb age of syn- and post-metamorphic granitoids of south Mongolia: evidence for the presence of grenvillides in the central asian foldbelt. Doklady Earth Sciences 404, 986–990.

Yarmolyuk, V.V., Kovalenko, V.I., Sal'nikova, E.B., Kovach, V.P., Kozlovsky, A.M., Kotov, A.B., Lebedev, V.I., 2008. Geochronology of igneous rocks and formation of the late paleozoic south Mongolian active margin of the siberian continent. Stratigraphy and Geological Correlation 16 (2), 162–181.

Yin, A., Nie, S., 1996. A Phanerozoic palinspastic reconstruction of China and its neighboring regions. In: Yin, A., Harrison, T.M. (Eds.), The Tectonic Evolution of Asia. Cambridge University Press, Cambridge, pp. 442–485.

Zhao, G.C., Sun, M., Wilde, S.A., Li, S.Z., Liu, S.W., Zhang, J., 2006. Composite nature of the north China granulite-facies belt: tectonothermal and geochronological constraints. Gondwana Research 9 (3), 337–348.

Zhao, G.C., Cawood, P.A., 2012. Precambrian geology of China. Precambrian Research 222–223, 13–54.

Zhao, P., Fang, J.Q., Xu, B., Chen, Y., Faure, M., 2014. Early paleozoic tectonic evolution of the Xing-meng orogenic belt: constraints from detrital zircon geochronology of western Erguna–Xing'an block, north China. Journal of Asian Earth Sciences 95, 136–146.

Zhang, J., Sun, M., Schulmann, K., Zhao, G.C., Wu, Q., Jiang, Y.D., Guy, A., Wang, Y.J., 2015a. Distinct deformational history of two contrasting tectonic domains in the Chinese Altai: their significance in understanding accretionary orogenic process. Journal of Structural Geology 73, 64–82.

Zhang, J.F., Pang, Q.B., Zhu, Q., Jin, C.Z., Liu, G.J., 2004. Zircon U–Pb dating of the Bayan Bold granite-porphyry in Inner Mongolia: the age of the host rock of the Bayan Bold gold deposit. Regional Geology of China 23, 189–192 (in Chinese with English abstract).

Zhang, S., Gao, R., Li, H., Hou, H., Wu, H., Li, Q., Yang, K., Li, C., Li, W., Zhang, J., Yang, T., Keller, G.R., Liu, M., 2014. Crustal structures revealed from a deep seismic reflection profile across the Solonker suture zone of the Central Asian orogenic belt, northern China: an integrated interpretation. Tectonophysics 612–613 (3), 26–39.

Zhang, X.H., Zhang, H.F., Tang, Y.J., Wilde, S.A., Hu, Z.C., 2008. Geochemistry of permian bimodal volcanic rocks from central Inner Mongolia, north China: Implication for tectonic setting and phanerozoic continental growth in central asian orogenic belt. Chemical Geology 249, 262–281.

Zhang, X.H., Wilde, S.A., Zhang, H.F., Zhai, M.G., 2011. Early Permian high-K calc-alkaline volcanic rocks from NW Inner Mongolia, North China: geochemistry, origin and tectonic implications. Journal of the Geological Society 168, 525–543.

Zhang, X.H., Yuan, L.L., Xue, F.H., Yan, X., Mao, Q., 2015b. Early Permian A-type granites from central Inner Mongolia, North China: magmatic tracer of post-collisional tectonics and oceanic crustal recycling. Gondwana Research 28 (1), 311–327.

Zhang, Z.C., Li, K., Li, J.F., Tang, W.H., Chen, Y., Luo, Z.W., 2015c. Geochronology and geochemistry of the eastern Erenhot ophiolitic complex: implications for the tectonic evolution of the Inner Mongolia-Daxinganling orogenic belt. Journal of Asian Earth Sciences 97, 279–293.

Zhou, J.B., Han, J., Zhao, G.C., Zhang, X.Z., Cao, J.L., Wang, B., Pei, S.H., 2015. The emplacement time of the Hegenshan ophiolite: constraints from the unconformably overlying Paleozoic strata. Tectonophysics 662, 398–415.

Zhou, W.X., 2012. Studies of Geochronology and Geochemistry of Paleozoic Magmatism in Xilinhot Area, Inner Mongolia. Ph.D. thesis. China University of Geosciences (in Chinese with English abstract).

Zhu, C.Y.L., Zhao, G.C., Sun, M., Liu, Q., Han, Y.G., Hou, W.Z., Zhang, X.R., Eizenhofer, P.R., 2015. Geochronology and geochemistry of the Yilan blueschists in the Heilongjiang Complex, northeastern China and tectonic implications. Lithos 216–217, 241–253.